

Asymptotic Analysis for Greedy Initialization of Threshold-Based Distributed Optimization of Persistent Monitoring on Graphs

Shirantha Welikala, *Student Member, IEEE*, and Christos G. Cassandras, *Fellow, IEEE*,

Abstract—We consider the optimal multi-agent persistent monitoring problem defined for a team of agents on a set of nodes (targets) interconnected according to a fixed graph topology. The objective is to minimize a measure of mean overall node state uncertainty evaluated over a finite time interval. In prior work, a class of distributed threshold-based parametric controllers has been proposed where agent dwell times at nodes and transitions from one node to the next are controlled by enforcing thresholds on the respective node uncertainties. Under such a threshold policy, on-line gradient-based techniques (such as the Infinitesimal Perturbation Analysis (IPA)) are then used to determine optimal threshold values. However, due to the non-convexity of the problem, this approach leads to often poor local optima highly dependent on the initial thresholds used. To overcome this initialization challenge, in this paper, the asymptotic steady-state behavior of the agent-target system is extensively analyzed. Based on the obtained theoretical results, a computationally efficient off-line greedy technique is developed to systematically generate initial thresholds. Extensive numerical results show that the initial thresholds provided by this greedy technique are almost immediately (locally) optimal or quickly lead to optimal values. In all cases, they perform significantly better than the locally optimal solutions known to date.

Index Terms—Multi-agent Systems, Hybrid Systems, Optimization, Trajectory Planning,

I. INTRODUCTION

A persistent monitoring problem arises when a dynamically changing environment needs to be monitored by a set of agents, who cannot effectively cover the environment if remained stationary. This constraint of having to have non-stationary exploratory agents to cover the changing environment contrasts persistent monitoring problems from conventional multi-agent coverage [1] and consensus [2] problems. In applications like sweep coverage and patrolling [3], [4], every point in the environment is equally valued for agents to cover. However, in many other applications, agent explorations on the changing environment should be focused around a finite set of “points of interest” which can be modeled as “data sources” or “targets” that needed to be monitored consistently. One such application is in surveillance systems [5], [6] where a set of valuable objects/regions in the environment needs to be visited constantly by a team of agents. Further, this

particular problem setting can also be seen in applications in environmental sensing [7], [8], data collecting [9], [10], [11], energy management [12] and also in particle tracking of nano-scale systems [13].

The problem considered in this paper is also focused only on a finite number of known data sources (called “targets”) located in the environment. In this setting, the goal of the agent team is to collect information from (also called “sense”) each target to reduce a metric (also called “uncertainty”) associated with the target state. The general behavior of a target uncertainty metric is such that it increases while no agent is present in the vicinity of the target, and, it decreases when the target is being sensed by one or more agents who are now in the vicinity. The sensing capabilities of agents are typically characterized by a sensing range and a sensing rate function which respectively defines the minimum proximity required to sense a target and the rendered rate of decrease in the sensed target uncertainty. Therefore, the underlying global objective is to minimize an overall measure of target uncertainties through controlling the agent trajectories/behaviors.

For a similar agent-target paradigm, the work in [9] (also in [8]) has addressed the persistent monitoring problem in a one-dimensional environment by formulating it as an optimal control problem and reducing it into a parametric optimization problem where the parameters are (i) locations where each agent has to switch its direction, and, (ii) the dwell time at each such switching point. For this case, these parameters are sufficient to characterize each agent’s optimal trajectory fully. Most importantly, this parametrization has enabled the use of Infinitesimal Perturbation Analysis (IPA) [14] to determine gradients of the interested objective function with respect to the parameters and to subsequently obtain optimal parameters (using gradient descent) which corresponds to the optimal agent trajectories.

However, for similar persistent monitoring problems in two-dimensional environments, the work in [4] has shown that the optimal agent trajectories cannot be represented in such simple parametric forms. As alternatives, number of different forms of parametric trajectories such as elliptical, Lissajous, Fourier, and interconnected-linear, have been proposed and used to obtain at least a near-optimal solution (i.e., a controller) [4], [11]. However, as first pointed out in [15], limiting the agent trajectories into such standard forms can lead to poor local optima as such solutions cannot capture the dynamic changes in target uncertainties or the effect of initial target/agent conditions [8], [4], [11].

*Supported in part by NSF under grants ECCS-1509084, DMS-1664644, CNS-1645681, by AFOSR under grant FA9550-15-1-0471, by ARPA-E’s NEXTCAR program under grant DE-AR0000796 and by the MathWorks.

Authors are with the Division of Systems Engineering and Center for Information and Systems Engineering, Boston University, Brookline, MA 02446, {shirant27, cgc}@bu.edu.

Manuscript received July 22, 2019; revised July 22, 2019.

To overcome the aforementioned challenges associated with the two-dimensional persistent monitoring problems, the work in [15] have taken a different approach by respectively abstracting the targets and the feasible inter-target agent trajectories as nodes and edges of a graph topology. This abstraction gives the added advantage of accounting for physical obstacles that might be present in the considered environment. In this paradigm, an agent trajectory can be fully characterized by a sequence of nodes to be visited and an associated dwell time to be spent at each visited node in the sequence. Therefore, the optimal controller which optimizes a given objective should yield such a (target, dwell-time) sequence for all the agents. Due to the complexity of a such optimization problem [16] (even when compared to traveling salesman problems [17]), the work in [15] have introduced a class of distributed threshold-based parametric controllers which characterize agent transitions from one node to the next based on enforcing thresholds on respective node uncertainties. This parametrization has enabled the use of IPA to find the optimal threshold parameters (hence the optimal controller, within the considered class of parametric controllers) in an on-line manner using gradient descent. However, due to the non-convexity of the associated objective function (with respect to the used threshold parameters), the optimal thresholds given by such a gradient approach is often sub-optimal and highly depends on the used initial thresholds - which in [15] have generated randomly.

In this paper, for the same persistent monitoring problem considered in [15], [18], we continue to improve upon the solution approach proposed in [15]. In particular, our primary focus is on finding a set of “favorable” initial thresholds to initiate the IPA based gradient descent process such that an improved set of optimal thresholds are obtained (still locally optimal). The proposing “initialization” process is designed to be applied in an offline manner with a minimal computational power.

It is reasonable to expect that if the agents are controlled according to a randomly generated set of thresholds, the performance of the persistent monitoring systems would be poor. This implies that using gradient descent with a randomly generated set of thresholds (like in [15]) is inherently a challenging task. Therefore, in this paper, we first seek to construct a high performing set of trajectories for the given set of agents on the given target topology (i.e., the graph). Then, we translate those identified agent trajectories into a corresponding set of thresholds. This formed set of thresholds is then used as the (favorable) initial thresholds in IPA based gradient descent. Thus, the resulting optimal set of thresholds should better than the optimal thresholds obtained with random initialization.

One of the main contributions of this paper is providing a computationally cheap, offline, greedy approach which is capable of constructing a high performing set of trajectories for a given set of agents on a given graph. Another crucial contribution of our work is providing a graph partitioning technique (can also be thought of as target clustering technique) for the persistent monitoring problems on graphs. We have also provided an extensive analysis on the asymptotic behavior

of single-agent persistent monitoring systems on graphs where the single agent is constrained to follow a periodic sequence of nodes (also known as a target-cycle) indefinitely. In conducted simulation examples, it was observed that the initial set of thresholds provided by the proposing technique is often locally optimal, thus, in such cases, it eliminates the need for a subsequent IPA based gradient descent process. Also, we have developed an interactive simulation interface (available at <http://www.bu.edu/codes/simulations/shiran27/PersistentMonitoring/>) where both the proposing solution technique in this paper and the solution technique proposed in [15] can be evaluated/compared for any generic problem configuration.

The paper is organized as follows. Section II provides the problem formulation and the solution technique proposed in [15]. Section III provides a technique to obtain an initial set of thresholds if the underlying graph is sufficiently dense, and if only one agent is being deployed. However, Section IV generalizes the concepts presented Section III by providing a technique to obtain an initial set of thresholds for any generic graph when only one agent is being deployed. Along the same lines, Section V further generalizes the proposing initialization technique for any generic graph under multi-agent situations. A sufficient number of simulation examples are discussed in each section, and, they have been compared with the respective state of the art solution [15]. Finally, Section VI provides the concluding remarks with a few interesting future research avenues.

II. PROBLEM FORMULATION

Consider a two-dimensional mission space with M targets (nodes) labeled $\mathcal{T} = \{1, 2, \dots, M\}$ and N agents labeled $\mathcal{A} = \{1, 2, \dots, N\}$. Each target $i \in \mathcal{T}$ is located at a fixed position $X_i \in \mathbb{R}^2$. Each agent $a \in \mathcal{A}$ is allowed to move in the mission space, therefore, its trajectory is denoted by $\{s_a(t) \in \mathbb{R}^2, t \geq 0\}$. Target locations and initial agent locations are prespecified.

Target Uncertainty Model: We follow the same model used in [15]. Each target $i \in \mathcal{T}$ has an associated *uncertainty state* $R_i(t) \in \mathbb{R}$ with the following properties: (i) $R_i(t)$ increases at a rate A_i when no agent is visiting it, (ii) $R_i(t)$ decreases at a rate $B_i N_i(t) - A_i$ where B_i is the uncertainty removal rate by an agent and $N_i(t) = \sum_{a=1}^N \mathbf{1}_{\{s_a(t)=X_i\}}$ is the number of agents present at target i at time t , and (iii) $R_i(t) \geq 0, \forall t \geq 0$. The target uncertainty state dynamics for any $i \in \mathcal{T}$ are

$$\dot{R}_i(t) = \begin{cases} 0 & \text{if } R_i(t) = 0 \text{ and } A_i \leq B_i N_i(t), \\ A_i - B_i N_i(t) & \text{otherwise,} \end{cases} \quad (1)$$

with, A_i, B_i and $R_i(0)$ values pre-specified. As pointed out in [15], this target uncertainty model has an attractive queueing system interpretation where each A_i and $B_i N_i(t)$ can be thought of as an arrival rate and a controllable service rate respectively for each target viewed as a node in a queueing network.

Agent Model: In some persistent monitoring models [9], each agent $a \in \mathcal{A}$ is assumed to have a finite sensing range $r_a > 0$ which allows it to decrease $R_i(t)$ whenever $\|s_a(t) - X_i\| \leq r_a$. However, we follow the approach used in [15] where $r_a = 0$ is assumed and $N_i(t)$ is used to represent the joint detection probability of a target $i \in \mathcal{T}$. This simplifies

the analysis and enables accommodation of the target graph topology [15].

As we will see next, contributions of this paper are invariant to the used dynamic model of the agents (partly due to the embedded graph model). Therefore, we do not explicitly state an agent model.

Objective function [15]: The objective of this persistent monitoring system is to minimize a measure of *mean system uncertainty* J_T (evaluated over a finite time horizon T), where

$$J_T = \frac{1}{T} \int_0^T \sum_{i=1}^M R_i(t) dt, \quad (2)$$

by controlling agent motion.

Target Topology (Graph): We embed a directed graph topology $\mathcal{G} = (\mathcal{V}, \mathcal{E})$ into the 2D mission space where the graph vertices represent the targets ($\mathcal{V} = \{1, 2, \dots, M\} = \mathcal{T}$), and the graph edges represent inter-target trajectory segments (which may be curvilinear paths with arbitrary shapes so as to account for potential obstacles in the mission space) available for agents to travel ($\mathcal{E} \subseteq \{(i, j) : i, j \in \mathcal{V}\}$). It is assumed that each edge $(i, j) \in \mathcal{E}$ has an associated fixed time value $\rho_{ij} \in \mathbb{R}_{\geq 0}$ which represents the amount of time that an agent has to spend to travel from target i to j . In general, ρ_{ij} may depend on the agent dynamic model, target locations and any obstacles that may present in the mission space. Also, we assume that if $(i, j) \in \mathcal{E}$, then, $(j, i) \in \mathcal{E}$ with $\rho_{ij} = \rho_{ji}$ (for simplicity only and no loss of generality). In this paradigm, the *neighbor set* \mathcal{N}_i of target i is defined as $\mathcal{N}_i = \{j : (i, j) \in \mathcal{E}\}$.

Under the assumed target dynamics in (1) and the agent sensing capabilities, it is intuitive that to minimize the objective J_T in (2) each agent has to dwell (i.e., remain stationary) only at each target that it visits in its trajectory. Further, according to the embedded target topology \mathcal{G} which constrains the agent motion, when an agent $a \in \mathcal{A}$ leaves a target $i \in \mathcal{V}$ after finishing its dwelling period, its next target would be some $j \in \mathcal{N}_i$. Therefore, agent a should continuously travel on the edge $(i, j) \in \mathcal{E}$ for a time duration ρ_{ij} to reach target j . It is clear that in order to minimize the objective J_T , the predefined ρ_{ij} ($= \rho_{ji}$) value should correspond to the minimum time an agent may take to travel between targets i and j . This *dwell-travel* approach is intended to minimize the agent time spent outside of targets (this is analogous to minimizing the idle time of service providers in a queueing network).

When an agent $a \in \mathcal{A}$ arrives at a target $i \in \mathcal{V}$, let this arrival time be t' . Now, the agent has to determine a *dwell time* $\tau_i^a \in \mathbb{R}_{\geq 0}$ and a *next visit target* $v_i^a \in \mathcal{N}_i$. After these two decisions are made, the same process repeats at the chosen next target (see Fig. 1). Therefore, the optimal approach to control the set of agents which minimizes the objective J_T in (2) can be determined in the form of a set of optimal dwelling time and next visit target sequences. This is a challenging task even for the simplest problem configurations due to the nature of the search space.

Threshold based control policy: Similar to the framework proposed in [15], we introduce a Threshold-based Control Policy (TCP). Under this TCP, each agent a bases its decision sequence by adhering to a set of pre-specified parameters denoted by $\Theta^a \in \mathbb{R}^{M \times M}$ which serve as thresholds

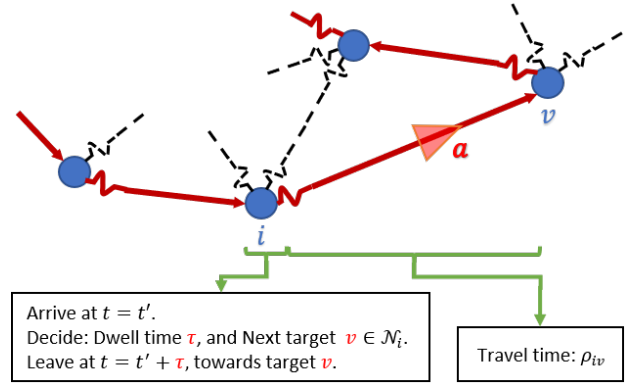


Fig. 1: Agent behavior defined by its decision sequence.

on the target uncertainties. Note that the $(i, j)^{\text{th}}$ parameter in the Θ^a matrix is denoted as $\theta_{ij}^a \in \mathbb{R}_{\geq 0} \forall i, j \in \mathcal{V}$.

Let us denote the set of neighbors of a target i which violate their thresholds (called *active neighbors*) when agent a is residing in i at time t by $\mathcal{N}_i^a(t) \subseteq \mathcal{N}_i$ where

$$\mathcal{N}_i^a(t) \triangleq \{j : R_j(t) > \theta_{ij}^a, j \in \mathcal{N}_i\}. \quad (3)$$

When agent a arrives at target i at time $t = t'$, the dwell time τ_i^a spent at target i is determined by: (i) the diagonal element θ_{ii}^a based on the threshold satisfaction condition $R_i(t) < \theta_{ii}^a$, and, (ii) the active neighbor existence condition $|\mathcal{N}_i^a(t)| > 0$ at $t = t' + \tau_i^a$ (where $|\cdot|$ is the cardinality operator). Subsequently, agent a 's next visit target v_i^a is chosen from the set of active targets $\mathcal{N}_i^a(t) \subseteq \mathcal{N}_i$ using the off-diagonal thresholds $\{\theta_{iv}^a : v \in \mathcal{N}_i^a(t)\}$ at $t = t' + \tau_i^a$. Formally,

$$\begin{aligned} \tau_i^a &:= \underset{\tau: \tau \geq 0}{\operatorname{argmin}} \{ [R_i(t' + \tau) < \theta_{ii}^a] \ \& \ [|\mathcal{N}_i^a(t' + \tau)| > 0] \}, \\ v_i^a &:= \underset{v: v \in \mathcal{N}_i^a(t' + \tau_i^a)}{\operatorname{argmax}} \{ R_v(t' + \tau_i^a) - \theta_{iv}^a \} \end{aligned} \quad (4)$$

These update equations when coupled with trivial $i := v_i^a$ and $t' := t' + \tau_i^a + \rho_{iv_i^a}$ updates, will define the (dwell time, next target) sequences of agents under the TCP.

The first condition in the τ_i^a expression in (4) ensures that agent a will dwell at target i until at least its own uncertainty $R_i(t)$ drops below θ_{ii}^a ; the second condition ensures that there exists at least one neighbor $v \in \mathcal{N}_i$ whose uncertainty $R_v(t)$ has increased beyond the threshold θ_{iv}^a . According to the v_i^a expression in (4), v_i^a is the neighboring target of i chosen from the set $\mathcal{N}_i^a(t' + \tau_i^a) \subseteq \mathcal{N}_i$ with the largest threshold violation.

It is important to point out that under this TCP based on (3) and (4), we limit agents from using non-neighboring target state information. This enables each agent to operate in a *distributed* manner using only the state information obtained from the target where it currently resides and from its neighboring targets. An example target topology and an agent threshold matrix are shown in Fig. 2. Notice that when certain edges are missing in the graph, the respective off-diagonal entries become irrelevant and are denoted by $\theta_{ij}^a = \infty$.

Discrete event system view: Under the described TCP, the behavior of the persistent monitoring system is fully defined by the set of agent decision sequences

$$\mathcal{U}(\Theta) = \{(\tau_{i(l)}^a(\Theta^a), v_{i(l)}^a(\Theta^a)) : a \in \mathcal{A}, i(l) \in \mathcal{V}, l = 1, 2, \dots\}.$$

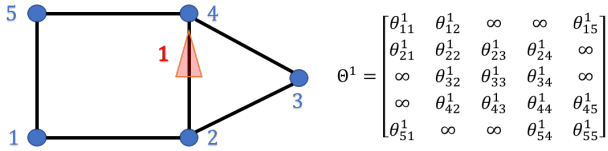


Fig. 2: An example target topology with five targets and one agent with its threshold parameters

Here, $\Theta \in \mathbb{R}^{M \times M \times N}$ is the collection of all agent threshold matrices and $i(l) \in \mathcal{V}$ is the l^{th} target visited by agent a .

Moreover, according to (4), the complete persistent monitoring system can be modelled as a discrete event system (DES), specifically as a *deterministic automata with outputs* [19]. In that case, the *state* would be the $N \times 2$ tuple with agent modes and their residing/pursuing target information. The *event set* is the set of: (i) all possible agent arrivals and departures at/from targets, (ii) the instances where a target uncertainty reaches 0 from above, and (iii) a ‘start’ and an ‘end’ events triggered only at times $t = 0$ and $t = T$ respectively. The *output* can be considered as a vector $\bar{R}^k = [R_i(t^k)]_{i \in \mathcal{V}} \in \mathbb{R}^M$ evaluated at all the event times $\{t^k : k \in \{0, 1, \dots, K\}\}$ with $t^0 = 0$ and $t^K = T$. Note that under some TCP Θ , we can get the state and output trajectories of the DES along with its event times by simulating (4).

Considering the dependence of both the state trajectory and the output trajectory on the chosen set of parameters Θ , the performance metric J_T in (2) depends on the parameters Θ . Therefore, within the TCP class of agent controllers, we aim at determining an Optimal TCP (OTCP) Θ^* such that

$$\Theta^* = \underset{\Theta \geq 0}{\operatorname{argmin}} J_T(\Theta) = \frac{1}{T} \sum_{i=1}^M \sum_{k=0}^K \int_{t^k}^{t^{k+1}} R_i(t) dt. \quad (5)$$

Differentiating the cost $J_T(\Theta)$ w.r.t. parameters Θ yields,

$$\nabla J_T(\Theta) = \frac{1}{T} \sum_{i=1}^M \sum_{k=0}^K \int_{t^k}^{t^{k+1}} \nabla R_i(t) dt. \quad (6)$$

where $\nabla \equiv \frac{\partial}{\partial \Theta}$. It should be noted that even though event times are dependent on the TCP Θ , when taking the derivative [20], the effect of it gets canceled out since we have fixed $t^0 = 0$ and $t^K = T$ [14]. Further, using the linear behavior of the target uncertainty dynamics in (1), and the way that we have designed our event space, following Lemma 1 in [15] we can easily show that $\nabla R_i(t) = \nabla R_i(t^k) \forall t \in (t^k, t^{k+1}]$. Therefore, the gradient $\nabla J_T(\Theta)$ becomes a simple summation:

$$\nabla J_T(\Theta) = \frac{1}{T} \sum_{i=1}^M \sum_{k=0}^K \nabla R_i(t^k) (t^{k+1} - t^k). \quad (7)$$

Previous work in [15]: In [15], where the class of TCP controllers was introduced, the use of Infinitesimal Perturbation Analysis (IPA) [14] is extensively discussed so as to evaluate $\nabla R_i(t^k)$ (hence, $\nabla J_T(\Theta)$) on-line and in a distributed manner. This enables the use of a gradient descent algorithm:

$$\Theta^{(l+1)} = \left[\Theta^{(l)} - \beta^{(l)} \nabla J_T(\Theta^{(l)}) \right]^+, \quad (8)$$

to update the TCP Θ iteratively. In (8), the projection operator $[\cdot]^+ = \max\{0, \cdot\}$ is used. The step size $\beta^{(l)}$ is selected such that

it diminishes according to the standard conditions $\sum_{l=1}^{\infty} \beta^{(l)} = \infty$ and $\lim_{l \rightarrow \infty} \beta^{(l)} = 0$ [21]. Note that each iteration l of (8) uses the data collected from a single trajectory (i.e., $\forall t \in [0, T]$) to evaluate $\nabla J_T(\Theta^{(l)})$.

The work in [15] uses a hybrid system model to construct realizations of this persistent monitoring system. However, in our formulation above, we have shown that it can be done via using a simple discrete event system model (4). The use of a DES model results in faster and efficient simulations and provides more intuition about the underlying decision making process. However, this modeling discrepancy will not affect any of our comparisons/conclusions made with respect to [15].

Initialization: $\Theta^{(0)}$: In [15] a randomly generated set of values is used to initialize thresholds $\Theta^{(0)}$ for (8). Due to the non-convexity of the objective function in (5), we expect that the resulting value of Θ when (8) converges depends on $\Theta^{(0)}$. Therefore, identifying well-performing initial thresholds will generally provide significant improvements over the local minimum resulting from randomly selected ones. Motivated by this idea, we first investigate the structural and behavioral properties of the underlying system (under a few additional constraints). That knowledge is then used to construct a candidate for $\Theta^{(0)}$.

Simulation results: In the ensuing discussion, we consider the problem configurations shown in Fig. 3(a) and Fig. 4(a) as running examples. In those diagrams, blue circles represent the targets while black lines represent available path segments that agents can take to travel between targets. Red triangles and the yellow vertical bars indicate the agent locations and the target uncertainty levels, respectively. Moreover, since both of those quantities are time-varying ($s_a(t)$ and $R_i(t)$), in figures we indicate their state at the terminal time $t = T$ in a simulation where the best TCP found Θ^* is used. Note that the problem configurations shown in Fig. 4(a) is a multi-agent situation with $N = 3$.

The Fig. 3(b) and Fig. 4(b) shows the evolution of $J_T(\Theta^{(l)})$ when the TCP $\Theta^{(l)}$ is updated according to (8) using gradients $\nabla J_T(\Theta^{(l)})$ given by the IPA method as proposed in [15]. The termination condition used for (8) is $\|\Theta^{(l+1)} - \Theta^{(l)}\|_{\infty} \leq \varepsilon$ where ε is a small positive number. If the termination condition occurs at the iteration $l = L$, then $\Theta^* = \Theta^{(L)}$ is used in generating the Fig. 3(a) and Fig. 4(a) as mentioned before.

The proposing persistent monitoring solution technique (discussed in the ensuing sections) including the method proposed in [15] were implemented in a JavaScript based simulator which is made available at

<http://www.bu.edu/codes/simulations/shiran27/PersistentMonitoring/>. Readers are invited to reproduce the reported results and also to try new problem configurations using the developed interactive simulator. It should be highlighted that all the problem parameters (numerical values) can be customized in the developed simulator.

In simulation examples used in this paper, numerical values of the underlying problem parameters have been chosen as follows. The target parameters were chosen as $A_i = 1$, $B_i = 10$ and $R_i(0) = 0.5$, $\forall i \in \mathcal{V}$. Also, the used target location coordinates (i.e., X_i) are specified in each problem configuration figure. Note that in all the examples, all the targets have been

placed inside a 600×600 mission space. The interested time period (i.e., the time horizon) was taken as $T = 500$. Each agent's maximum speed was taken as 50 units per second. The initial locations of the agents were chosen such that they are uniformly distributed among the targets at $t = 0$ (i.e., $s_a(0) = X_i$ with $i = 1 + (a - 1) * \text{round}(M/N)$). In cases where the initial TCP $\Theta^{(0)}$ is randomly generated, each finite element in $\Theta^{(0)}$ matrices is chosen from uniform random distribution $\text{unif}(0,10)$. Also, when using the gradient descent in (8), diminishing step sizes $\beta^{(l)} = \frac{0.25}{\sqrt{l}}$ was used.

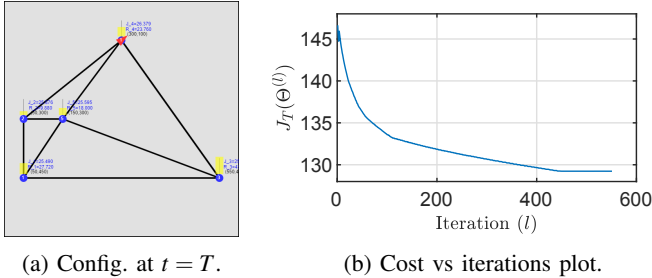


Fig. 3: Single agent simulation example 1 (SASE1): Starting with a random $\Theta^{(0)}$, converged to a TCP with the cost $J_T = 129.2$.

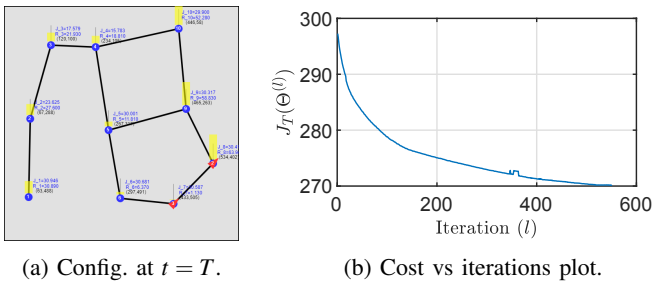


Fig. 4: Multi-agent simulation example 1 (MASE1): Starting with a random $\Theta^{(0)}$, converged to a TCP with the cost $J_T = 270.2$.

III. CYCLIC PERSISTENT MONITORING ON SUFFICIENTLY DENSE GRAPHS WITH 1 AGENT

Main conclusions of [15]: It is proved in [15] that in a single-agent persistent monitoring system it is optimal to make the target uncertainty $R_i(t) = 0$ on each visit of agent a at target i . In other words, in the OTCP, $\theta_{ii}^a = 0$. Moreover, experimental results in [15] provide some intuition about better performing agent behaviors: (i) after a brief initial transient phase, each agent converges to a (steady-state) periodic behavior where it cycles across a fixed subset of targets, and, (ii) in this steady state, agents do not tend to share targets with other agents.

Our approach: We now aim to use the aforementioned observations to efficiently construct better performing (favorable) agent trajectories which can be used to initialize the TCP allowing the gradient descent scheme (8) to achieve much better performance compared to random initialization approach used in [15]. Such trajectories take the form of a *target-cycle* on the given graph. Therefore, we need to

construct a set of target-cycles (one per agent) in the given graph topology.

In this section, as a starting point (and to make the problem tractable), we only focus on single-agent persistent monitoring problems on *sufficiently dense* target topologies. More precisely, we consider a given target topology $\mathcal{G} = (\mathcal{V}, \mathcal{E})$ to be a ‘sufficiently dense’ graph, if \mathcal{G} is *bi-triangular*. We formally define the concept of bi-triangularity in Definition 1.

Definition 1. A directed graph (take $\mathcal{G} = (\mathcal{V}, \mathcal{E})$) with $|\mathcal{V}| > 3$ is *bi-triangular* if for all $(i, j) \in \mathcal{E}$ there exists $k, l \in \mathcal{V}$ such that $(i, k), (k, j) \in \mathcal{E}$, $(i, l), (l, j) \in \mathcal{E}$, and $k \neq l$.

The following assumption formally states the conditions we assume in the analysis given in this section. However, it is worth mentioning that, in the forthcoming sections we will completely relieve this assumption.

Assumption 1. Consider that,

- 1) only one agent is available, and,
- 2) the given target topology $\mathcal{G} = (\mathcal{V}, \mathcal{E})$ is bi-triangular.

Under this Assumption 1, we only search for a single target-cycle (agent trajectory) in the given graph \mathcal{G} . Moreover, exploiting the assumed dense nature of the given graph, we propose an iterative greedy scheme to construct a high performing target-cycle. This constructed agent trajectory is then transformed to a TCP as $\Theta^{(0)}$ for the subsequent use in gradient descent (8) to obtain an OTCP Θ^* .

A. Analysis of a unconstrained target-cycle

A *target-cycle* is a finite sequence of targets selected from the given graph \mathcal{G} such that the corresponding sequence of edges also exist in \mathcal{E} . The latter condition enables an agent to traverse on such a target-cycle. An *unconstrained target-cycle* is a target-cycle with no target on it being repeated. We define the set \mathcal{C} to include all possible unconstrained target-cycles on the graph \mathcal{G} . A generic element of \mathcal{C} (i.e., a generic target-cycle) is denoted by $\Xi_i = \{i_1, i_2, \dots, i_m\} \subseteq \mathcal{V}$, where $i_j \in \mathcal{V}$, $j \in \{1, 2, \dots, m\}$ and $m = |\Xi_i| \leq M$. The corresponding sequence of edges are denoted by $\xi_i = \{(i_m, i_1), (i_1, i_2), \dots, (i_{m-1}, i_m)\} \subseteq \mathcal{E}$. Note that ξ_i is fully defined by Ξ_i , and, vice versa.

Since we are interested in greedily constructing a target-cycle with a high-performing mean system uncertainty value (i.e., J_T in (2)), we need to have an assessment criterion for any given arbitrary target-cycle. Thus, we define the *steady-state mean cycle uncertainty metric* $J_{ss}(\Xi_i)$,

$$J_{ss}(\Xi_i) = \lim_{T \rightarrow \infty} \frac{1}{T} \int_0^T \sum_{j \in \Xi_i} R_j(t) dt. \quad (9)$$

We now present an off-line (i.e., without executing sample paths of the system) technique to evaluate $J_{ss}(\Xi_i)$ based only on knowledge of the system model/parameters. Without loss of generality, for notational convenience, Ξ_i and its targets are relabeled as $\Xi = \{1, 2, \dots, n, n+1, \dots, m\}$ by dropping the subscript i (see Fig. 5). We make the following assumption regarding an agent's behavior on a target-cycle.

Assumption 2. After visiting a target $n \in \Xi$, an agent will leave it if and only if the target uncertainty reaches zero.

Here, the ‘only if’ component follows from the aforementioned result in [15] that it is optimal to make the target uncertainty $R_i(t) = 0$ whenever the agent visits target i . The ‘if’ component restricts agent decisions by assuming the existence of an active neighbor to i as soon as when $R_i(t) = 0$ occurs in (4). Nonetheless, recalling that our focus is only on initializing (8), this potential sub-optimality will be compensated by the eventual use of (8).

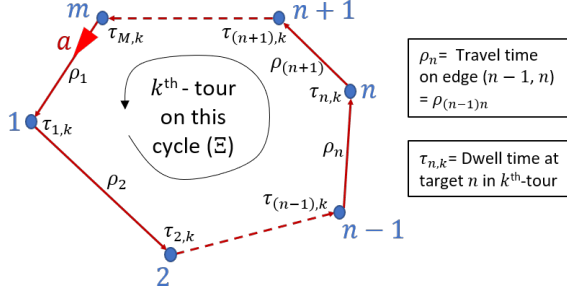


Fig. 5: A generic single agent unconstrained cycle Ξ .

A *tour* on the target-cycle Ξ (shown in Fig. 5) starts/ends when the agent leaves the last target m to reach target 1. When the agent a is in its k^{th} tour on Ξ , the dwell time spent at a target n is denoted by $\tau_{n,k}^a$ and the travel time spent on an edge $(n-1, n) \in \mathcal{E}$ is (by definition) $\rho_{(n-1)n}$. However, we respectively use $\tau_{n,k}$ and ρ_n to represent these two quantities as it does not introduce any ambiguity (note that $\rho_1 = \rho_{m1}$). Observe that travel times ρ_n are independent of k due to the embedded graph topology. Also, target n 's uncertainty level at the end of the k^{th} tour is denoted by $R_{n,k}$. Under this notation, the trajectories of target uncertainties $R_m(t)$ and $R_n(t)$ over k^{th} and $(k+1)^{\text{th}}$ tours are shown in Fig. 6.

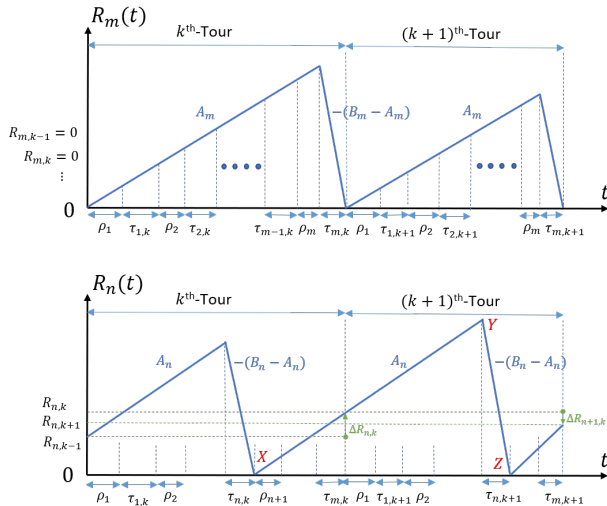


Fig. 6: Variation of target uncertainties during agent tours.

Using the XYZ triangle in the $R_n(t)$ trajectory shown in Fig. 6, the dynamics of target n 's dwell time $\tau_{n,k}$ (w.r.t. k , where

$n \in \Xi$) can be obtained as

$$(B_n - A_n)\tau_{n,k+1} = A_n \left(\sum_{i=n+1}^m [\rho_i + \tau_{i,k}] + \sum_{i=1}^{n-1} [\rho_i + \tau_{i,k+1}] + \rho_n \right) \quad (10)$$

Taking

$$\alpha_n \triangleq \frac{B_n - A_n}{A_n}, \quad (11)$$

and setting $\rho_\Xi = \sum_{i=1}^m \rho_i$ to be the total cycle travel time, the above relationship (10) can be simplified into the form

$$-\sum_{i=1}^{n-1} \tau_{i,k+1} + \alpha_n \tau_{n,k+1} = \rho_\Xi + \sum_{i=n+1}^m \tau_{i,k}. \quad (12)$$

Now, (12) can be written for all $n \in \Xi$ in a compact form using the vectors $\bar{\tau}_k = [\tau_{1,k}, \tau_{2,k}, \dots, \tau_{m,k}]^T$, $\bar{\alpha} = [\alpha_1, \alpha_2, \dots, \alpha_m]^T$ and $\bar{1}_m = [1, 1, \dots, 1]^T \in \mathbb{R}^m$, as,

$$\Delta_1 \bar{\tau}_{k+1} = \Delta_2 \bar{\tau}_k + \bar{1}_m \rho_\Xi, \quad (13)$$

where $\Delta_2 \in \mathbb{R}^{m \times m}$ is the strictly upper triangular matrix with all non zero elements being 1, and, $\Delta_1 = \text{diag}(\bar{\alpha}) - \Delta_2^T$. The expression in (13) describes the evolution of agent's dwell times at all the targets on the cycle Ξ over the number of tours completed k . Note that it takes the format of an affine linear system.

In order to get an explicit expression for the mean steady state cycle uncertainty $J_{ss}(\Xi)$ given in (9) we first need to establish following three lemmas.

Lemma 1. (Shermon-Morrison lemma, [22]) Suppose $A \in \mathbb{R}^{m \times m}$ is an invertible matrix and $u, v \in \mathbb{R}^{m \times 1}$ are vectors. Then, $\det(A + uv^T) = (1 + v^T A^{-1} u) \det(A)$, and,

$$(1 + v^T A^{-1} u) \neq 0 \iff (A + uv^T)^{-1} = A^{-1} - \frac{A^{-1} uv^T A^{-1}}{1 + v^T A^{-1} u}.$$

Lemma 2. When $\sum_{i=1}^m \frac{A_i}{B_i} < 1$, the system of equations given in (13) has a feasible equilibrium point $\bar{\tau}_{eq}$ (reached at $k = k_{eq}$),

$$\bar{\tau}_{eq} = \left(\frac{\bar{\beta}}{1 - \bar{1}_m^T \bar{\beta}} \right) \rho_\Xi, \quad \text{i.e., } \tau_{n,k_{eq}} = \left(\frac{\beta_n}{1 - \sum_{i=1}^m \beta_i} \right) \rho_\Xi, \quad (14)$$

for all $n \in \Xi$ with

$$\beta_n \triangleq \frac{A_n}{B_n} \quad (15)$$

and $\bar{\beta} = [\beta_1, \beta_2, \dots, \beta_m]^T$.

Proof. At $k = k_{eq}$, in (13), $\bar{\tau}_{k+1} = \bar{\tau}_k = \bar{\tau}_{eq}$. Therefore,

$$\bar{\tau}_{eq} = (\Delta_1 - \Delta_2)^{-1} \bar{1}_m \rho_\Xi. \quad (16)$$

Using $\Delta_1 = \text{diag}(\bar{\alpha}) - \Delta_2^T$ and $\text{diag}(\bar{1}_m) + \Delta_2^T + \Delta_2 = \bar{1}_m \bar{1}_m^T$,

$$\bar{\tau}_{eq} = (\text{diag}(\bar{\alpha} + \bar{1}_m) - \bar{1}_m \bar{1}_m^T)^{-1} \bar{1}_m \rho_\Xi. \quad (17)$$

The expressions used for α_n and β_n gives that $(\alpha_n + 1) = 1/\beta_n$. Therefore, $(\text{diag}(\bar{\alpha} + \bar{1}_m))^{-1} = \text{diag}(\bar{\beta})$. Also, note that

$\text{diag}(\bar{\beta})\bar{I}_m = \bar{\beta}$ and $I_m \in \mathbb{R}^{m \times m}$ is an identity matrix. Now, using Lemma 1,

$$\begin{aligned}\bar{\tau}_{eq} &= \text{diag}(\bar{\beta}) \left(I_m + \frac{\bar{I}_m \bar{I}_m^T \text{diag}(\bar{\beta})}{1 - \bar{I}_m^T \bar{\beta}} \right) \bar{I}_m \rho_{\Xi}, \\ &= \text{diag}(\bar{\beta}) \left(\bar{I}_m + \frac{\bar{I}_m \bar{I}_m^T \bar{\beta}}{1 - \bar{I}_m^T \bar{\beta}} \right) \rho_{\Xi}, \\ \therefore \bar{\tau}_{eq} &= \left(\frac{\bar{\beta}}{1 - \bar{I}_m^T \bar{\beta}} \right) \rho_{\Xi}.\end{aligned}\quad (18)$$

Components of $\bar{\tau}_{eq}$ are non-negative only when $1 - \bar{I}_m^T \bar{\beta} > 0$. Thus, using the definition of $\bar{\beta}$, we get $\bar{I}_m^T \bar{\beta} = \sum_{i=1}^m \frac{A_i}{B_i} < 1$. \square

In order to establish the stability properties of $\bar{\tau}_{eq}$ given by the Lemma 2, we need make the following assumption.

Assumption 3. *The matrix $\Delta_1^{-1} \Delta_2$ is Schur stable [23].*

We point out that all the eigenvalues of Δ_2 are located at the origin as it is a strictly upper triangular matrix. Further, since Δ_1 is a lower triangular matrix with diagonal elements being $\{\alpha_i : i \in \Xi\}$, the eigenvalues of Δ_1^{-1} are located at $\{\frac{1}{\alpha_i} : i \in \Xi\}$. Using the definition of $\alpha_i (= \frac{B_i - A_i}{A_i})$, it is easy to show that $|\frac{1}{\alpha_i}| < 1 \iff 0 \leq \frac{A_i}{B_i} < \frac{1}{2}$, which is less restrictive than the condition $\sum_{i=1}^m \frac{A_i}{B_i} < 1$ required in Lemma 2. Therefore, it seems reasonable to conjecture that the eigenvalues of $\Delta_1^{-1} \Delta_2$ are located within the unit circle; however, to date, we have not provided a formal proof to the statement in Assumption 3.

Lemma 3. *Under the Assumption 3, the equilibrium point $\bar{\tau}_{eq}$ given in Lemma 2 for the affine linear system (13) is globally asymptotically stable.*

Proof: Let $\bar{e}_k = \bar{\tau}_k - \bar{\tau}_{eq}$ as the steady state error. Then, we can write $\bar{e}_{k+1} = \bar{\tau}_{k+1} - \bar{\tau}_{eq}$ and using (13) and Lemma 2,

$$\begin{aligned}\bar{e}_{k+1} &= (\Delta_1^{-1} \Delta_2 \bar{\tau}_k + \Delta_1^{-1} \bar{I}_m \rho_{\Xi}) - (\Delta_1^{-1} \Delta_2 \bar{\tau}_{eq} + \Delta_1^{-1} \bar{I}_m \rho_{\Xi}), \\ \therefore \bar{e}_{k+1} &= \Delta_1^{-1} \Delta_2 \bar{e}_k.\end{aligned}\quad (19)$$

Therefore, under Assumption 3, all the eigenvalues of $\Delta_1^{-1} \Delta_2$ are within the unit circle. Thus, the equilibrium point $\bar{\tau}_{eq}$ given in (14) of (13) is globally asymptotically stable [23]. (i.e., $\lim_{k \rightarrow \infty} \bar{\tau}_k = \bar{\tau}_{eq}$, irrespective of $\bar{\tau}_0$). \blacksquare

We now present our main theorem regarding the mean steady state cycle uncertainty in (9) achieved for the persistent monitoring system shown in Fig. 5.

Theorem 1. *Under Assumptions 2 and 3 with $\sum_{i=1}^m \frac{A_i}{B_i} < 1$, the single agent unconstrained target-cycle persistent monitoring configuration shown in Fig. 5 achieves a steady state mean cycle uncertainty value (i.e., $J_{ss}(\Xi)$ defined in (9)),*

$$J_{ss}(\Xi) = \frac{1}{2} (\bar{B} - \bar{A})^T \bar{\tau}_{ss}, \quad (20)$$

where $\bar{B} = [B_1, B_2, \dots, B_m]^T$, $\bar{A} = [A_1, A_2, \dots, A_m]^T$, and $\bar{\tau}_{eq}$ is given in (14).

Proof. Under the given conditions, both Lemma 2 and Lemma 3 apply. Therefore, using (9) we can write,

$$J_{ss}(\Xi) = \lim_{T \rightarrow \infty} \frac{1}{T} \int_0^T \sum_{n=1}^m R_n(t) dt = \frac{1}{T_{\Xi}} \int_{\partial T_{\Xi}} \sum_{n=1}^m R_n(t) dt, \quad (21)$$

where, $T_{\Xi} \triangleq \rho_{\Xi} + \bar{I}_m^T \bar{\tau}_{eq}$ is the *steady state tour duration* and ∂T_{Ξ} is a time period corresponding to a tour occurring after achieving the steady state. This can be further simplified into

$$J_{ss}(\Xi) = \sum_{n=1}^m \frac{1}{T_{\Xi}} \int_{\partial T_{\Xi}} R_n(t) dt. \quad (22)$$

Now, using the $R_n(t)$ trajectory shown in Fig. 6 note that when the equilibrium is achieved (as $T \rightarrow \infty \implies k \rightarrow \infty$), the final tour uncertainties will remain stationary (i.e., $R_{n,k} = R_{n,k+1}, \forall n \in \Xi$). As a result, the area under the $R_n(t)$ trajectory evaluated over a period T_{Ξ} becomes equivalent to that of a triangle where the base is T_{Ξ} and the height is $(B_n - A_n) \tau_{n,\infty}, \forall n \in \Xi$. Therefore,

$$\begin{aligned}J_{ss}(\Xi) &= \sum_{n=1}^m \frac{1}{T_{\Xi}} \frac{1}{2} T_{\Xi} (B_n - A_n) \tau_{n,\infty}, \\ \therefore J_{ss}(\Xi) &= \frac{1}{2} (\bar{B} - \bar{A})^T \bar{\tau}_{ss},\end{aligned}\quad (23)$$

where $\bar{\tau}_{\infty} = \bar{\tau}_{ss} = \bar{\tau}_{eq}$ given in Lemma 2. \square

Theorem 1 provides a means of assessing simple persistent monitoring configurations (like the one shown in Fig. 5) without having to simulate them. We will next discuss the usage of Theorem 1 in constructing a better performing target-cycle - on the given target topology \mathcal{G} .

B. Sub-optimal target-cycle construction via a greedy scheme

Under Assumption 1 for the given target topology \mathcal{G} , if $|\mathcal{C}|$ is small, Theorem 1 can be used to directly identify the best performing (steady state) target-cycle via brute-force search:

$$\Xi^* = \arg \min_{\Xi \in \mathcal{C}} J_{ss}(\Xi). \quad (24)$$

However, such a brute-force approach is often computationally exhaustive as $|\mathcal{C}|$ grows exponentially with respect to the number of targets in the graph \mathcal{G} (i.e., $|\mathcal{V}|$). In such situations, a computationally efficient alternative is to construct a (sub-optimal) target-cycle according to a greedy scheme. Typically, an iteration of such a greedy scheme will search to expand a set variable: *current target-cycle* (say Ξ) by adding an unvisited target $i \in \mathcal{V} \setminus \Xi$ to it. Here \setminus represents the set subtraction operation.

In this work, we follow the aforementioned greedy approach to construct a sub-optimal target-cycle, and then we derive the set of corresponding threshold control policy values as a candidate for the $\Theta^{(0)}$ for the use in (8). Therefore, getting the optimal target-cycle Ξ^* is not a necessity at this stage when compared to the importance of keeping the overall process of getting a candidate for $\Theta^{(0)}$ efficient and offline.

Before getting into the details of the proposing greedy scheme, we need to make an assumption and two more lemmas.

Estimating finite horizon objective J_T : Let us define the finite horizon version of $J_{ss}(\Xi_i)$ function (originally defined in (9) for a generic target-cycle $\Xi_i = \{i_1, i_2, \dots, i_m\} \subseteq \mathcal{V}$) as the *finite horizon mean cycle uncertainty* $J_T(\Xi_i)$, where,

$$J_T(\Xi_i) = \frac{1}{T} \int_0^T \sum_{j: j \in \Xi_i} R_j(t) dt. \quad (25)$$

Note that this $J_T(\Xi_i)$ metric is equivalent to the mean system uncertainty metric J_T defined in (2), when evaluated considering only the targets in set Ξ_i (i.e., when $\mathcal{V} = \Xi$).

Contribution of a neglected target: Formally, a **neglected target** is a target which is not visited by an agent during the time period $[0, T]$. Given the finite horizon nature of the objective function J_T in (2), if one (or few) target is located remotely compared to the rest of the targets, then neglecting such a remote target might be better than trying to cover it. Following lemma investigates the contribution of such neglected targets to the objective J_T .

Lemma 4. *The contribution of a neglected target $i \in \mathcal{V}$ to the mean system uncertainty J_T (defined in (2)) is $\left(R_{i,0} + \frac{A_i T}{2}\right)$.*

Proof. Consider the original problem configuration where we had M targets: $\mathcal{V} = \{1, 2, \dots, M\}$. Under this setting, the mean system uncertainty J_T defined in (2) can be decomposed as,

$$\begin{aligned} J_T &= \frac{1}{T} \int_0^T \sum_{j: j \in \mathcal{V}} R_j(t) dt \\ &= \frac{1}{T} \int_0^T \sum_{j: j \in \mathcal{V} \setminus \{i\}} R_j(t) dt + \frac{1}{T} \int_0^T R_i(t) dt \end{aligned}$$

Therefore, the second term above represents the contribution of the target i to the overall objective J_T . However, since target i is not being visited by an agent during $t \in [0, T]$, $\dot{R}_i(t) = A_i \forall t \in [0, T]$. Also note that the initial target uncertainty of i is $R_{i,0}$. Therefore, the contribution of target i can be simplified as

$$\frac{1}{T} \int_0^T R_i(t) dt = \frac{1}{T} \int_0^T R_{i,0} + A_i t dt = \left(R_{i,0} + \frac{A_i T}{2}\right).$$

□

Assumption 4. *For any target-cycle $\Xi \in \mathcal{C}$, the difference between the steady state mean cycle uncertainty $J_{ss}(\Xi)$ (in (9)) and the finite horizon mean cycle uncertainty $J_T(\Xi)$ (in (25)) is bounded by some finite constant $K_e \in \mathbb{R}_{\geq 0}$. In other words,*

$$|J_{ss}(\Xi) - J_T(\Xi)| < K_e. \quad (26)$$

In the presenting greedy scheme, we use the $J_{ss}(\cdot)$ metric in (9) to compare the performance of different target-cycles as it can be efficiently evaluated using theorem (1). However, since we originally have a finite horizon global objective as in (2), the $J_T(\cdot)$ metric defined in (25) is the most accurate measure to evaluate target-cycle performances. This assumption states that $J_T(\cdot)$ should always lie within $J_{ss}(\cdot) \pm K_e$. Following facts can be highlighted regarding this estimation error.

- 1) It is small when the steady state tour duration $T_{\Xi} (\triangleq \rho_{\Xi} + \bar{\Gamma}_m^T \bar{\tau}_{eq})$ and the finite horizon T is such that: $T \gg T_{\Xi}$.
- 2) It is small if the dynamics of steady state error of (13) are faster (i.e., according to (3), when $0 \simeq \frac{A_i}{B_i} \ll 1$).

Target-cycle expansion operation: Recall that we used the notation $\Xi_i = \{i_1, i_2, \dots, i_m\}$ to represent a generic target-cycle and $\xi_i = \{(i_m, i_1), (i_1, i_2), \dots, (i_{m-1}, i_m)\}$ to represent the respective sequence of edges in the target-cycle Ξ_i .

Omitting the subscript i (for notational convenience) consider a situation where we have a target-cycle $\Xi = \{1, 2, \dots, m\}$ with its respective edge set $\xi = \{(m, 1), (1, 2), \dots, (m-1, m)\}$. Now, to expand Ξ so that it includes one more target i picked from the set of neglected targets $\mathcal{V} \setminus \Xi$, we have to: (i) remove one edge chosen from ξ and replace it with two new consecutive edges, and (ii) place target i inside Ξ according to the conducted edge replacement. These two operations will define a new (expanded) target-cycle Ξ' (and ξ') as shown in Fig. 7. Following lemma investigates the estimated gain in the objective function due to such a target-cycle expansion. This gain is formally called as the *marginal gain* and is denoted by $\Delta J_T(i|\xi, e)$.

Theorem 2. *Under Assumptions 1, 2 and 4, the estimated gain (reduction) in the objective function J_T due to the target-cycle expansion operation (shown in Fig. 7) is*

$$\Delta J_T(i|\xi, (n-1, n)) = \left(R_{i,0} + \frac{A_i T}{2}\right) + J_{ss}(\Xi) - J_{ss}(\Xi'). \quad (27)$$

Here, Ξ' is the expanded cycle and $J_{ss}(\cdot)$ is from Theorem 1. The associated estimation error of this term would be $\pm 2K_e$.

Proof. When the target i is neglected, using Lemma 4, the mean system uncertainty (i.e., of the targets Ξ and i) is,

$$\left(R_{i,0} + \frac{A_i T}{2}\right) + J_T(\Xi).$$

After the target-cycle expansion, the mean system uncertainty would be $J_T(\Xi')$. Note that now $i \in \Xi'$ and $J_T(\cdot)$ is defined in (25). Therefore, the actual gain (reduction) in the objective function J_T would be,

$$\left(R_{i,0} + \frac{A_i T}{2}\right) + J_T(\Xi) - J_T(\Xi').$$

Now, under the Assumption 4, above quantity can be estimated (with a tolerance of $\pm 2K_e$) by the introduced marginal gain function in (27),

$$\Delta J_T(i|\xi, (n-1, n)) = \left(R_{i,0} + \frac{A_i T}{2}\right) + J_{ss}(\Xi) - J_{ss}(\Xi').$$

□

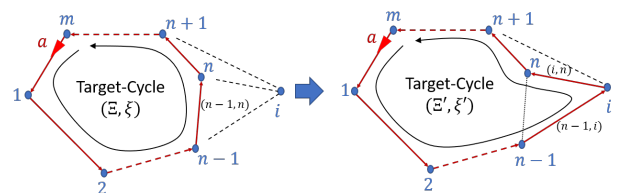


Fig. 7: A basic cycle expanding operation.

Greedy algorithm: Now, we propose the following greedy scheme (Algorithm 1) as a means of constructing a sub-optimal target-cycle for (24) under the given target topology. It starts from searching for the best target-cycle of length 2 (i.e. $\Xi \ni |\Xi| = 2$). The search space length is $|\mathcal{E}|$ and the obtained solution is then used as the initial target-cycle. Next, the current target-cycle is iteratively expanded by adding an external targets sequentially. The step 6 of algorithm decides the target to be added (and the edge to be removed) via brute-force search. In the k^{th} target-cycle expansion step, if \mathcal{G} is fully connected, the search space length is $(k+1) \times (|\mathcal{V}| - k - 1)$, where $(k+1)$ is the number of edges in the current target-cycle and $(|\mathcal{V}| - k - 1)$ is the number of remaining neglected targets available. Thus, the search space size remains moderate through greedy iterations.

TSP inspired target-cycle refinements: The underlying idea behind Algorithm 1 can be seen as a heuristic tour construction approach for an initial solution to the Traveling Salesman Problem (TSP) on \mathcal{G} [24]. However, there are two fundamental differences in our problem setup compared to a TSP: both the marginal gain function in Theorem 2 and the tour cost function in Theorem 1 are much more complex. In a TSP, these two functions would be simple distance-based metrics. Moreover, compared to TSPs, in persistent monitoring, a cost value, i.e., $J_{ss}(\cdot)$, cannot be assigned to individual edges of the topology, but can only be assigned to target-cycles using Theorem 1.

This compatibility with TSP raises an important question: “Can’t we adopt heuristic tour construction methods used in TSP to replace Algorithm 1?” The answer is: It is not possible, because, in persistent monitoring, we cannot assign a cost value to individual edges of the topology separately, we only can assign a cost (using Theorem 1) for target-cycles.

However, once we constructed a sub-optimal target-cycle (Let us denote by $\Xi^{\#}$) using Algorithm 1, we can adopt local search (also called local perturbation or tour improvement) techniques introduced in TSP literature. Specifically, we use the conventional *2-Opt* and *3-Opt* techniques [25], [24] to further refine the obtained $\Xi^{\#}$. The main idea behind a step of these methods is to slightly perturb (See Fig. 8) the shape of $\Xi^{\#}$ (say into Ξ') and then to see whether $J_{ss}(\Xi') < J_{ss}(\Xi^{\#})$. If so, the update $\Xi^{\#} := \Xi'$ is used.

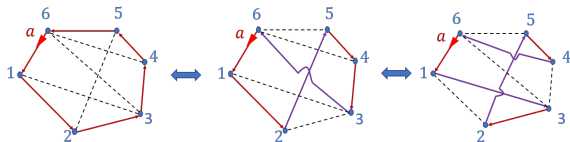


Fig. 8: A target-cycle and a possible 2-Opt move and a 3-Opt move (left to right).

C. The initial set of threshold control policy values: $\Theta^{(0)}$

Let us denote the obtained refined sub-optimal target-cycle as Ξ^R (and ξ^R). Now, we need to convert Ξ^R into a set of threshold control policy (TCP) values: $\Theta^{(0)}$ so that it can be used in (8) as the initial condition.

First, note that under Assumption 1, we only have one agent (i.e., $\mathcal{A} = \{a\}$). Therefore, essentially, $\Theta = \Theta^a \in \mathbb{R}^{M \times M}$. Then, notice that the TCP values in $\Theta^{a(0)}$ should guide the agent a according to the assumptions made in Assumption 2. Therefore, we can directly deduce a requirement: diagonal entries of $\Theta^{a(0)}$ should be 0. This will make sure that the agent a will stay till $R_i(t) = 0$ when it visited the target $i \in \Xi^R$ (See (4)). Next, we need to make sure that under the TCP values $\Theta^{a(0)}$ the agent will follow the intended cyclic trajectory Ξ^R . This can be achieved by setting $(i, j)^{\text{th}}$ entry of $\Theta^{a(0)}$ matrix to 0 for all $(i, j) \in \xi^R$. All the other (valid) entries of $\Theta^{a(0)}$ matrix should be chosen as $P \in \mathbb{R}$ where $P > T_{\Xi^R} \max_i A_i$ so that agent will remain in the same target-cycle Ξ^R . Algorithm 2 outlines this process and an example case is shown in Fig. 9.

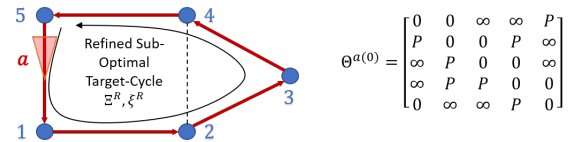
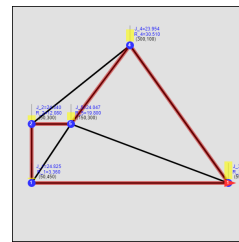
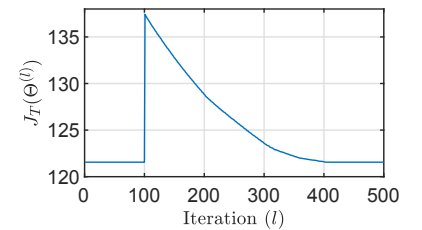


Fig. 9: The generated threshold matrix (right) for the refined sub-optimal target-cycle Ξ^R shown (left).

D. Simulation results

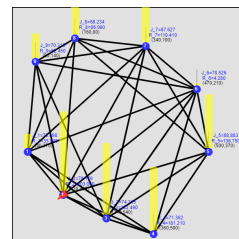


(a) Config. at $t = T$.

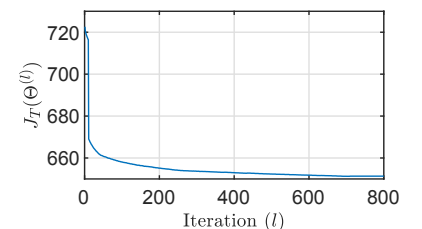


(b) Cost vs iterations plot.

Fig. 10: SASE1: The TCP $\Theta^{(0)}$ given by the identified cycle Ξ^R (the red trace in (a)) shows local optimality. At $l = 100$, $\Theta^{(l)}$ is randomly perturbed. Yet, converges back to the initial TCP. Cost $J_T = 121.6$ (Improvement = +7.6 compared to Fig. 3).



(a) Config. at $t = T$.



(b) Cost vs iterations plot.

Fig. 11: Single agent simulation example 2 (SASE2): Starting with a random $\Theta^{(0)}$, converged to a TCP with the cost $J_T = 651.3$.

Fig. 13 (a)→(d) shows the intermediate cycles generated by the greedy sub-optimal cycle construction process given

Algorithm 1 The proposing greedy algorithm for sub-optimal target-cycle construction under assumptions 1, 2 and 4.

```

1: Input: Target topology  $\mathcal{G} = (\mathcal{V}, \mathcal{E})$ , where,  $\mathcal{V} = \{1, 2, \dots, M\}$ , and,  $\mathcal{E} = \{(j, l) : j, l \in \mathcal{V}\}$ .
2: Output: A sub-optimal target-cycle  $\Xi^\#$  (and  $\xi^\#$ ).
3:  $(j^*, l^*) := \underset{(j, l) \in \mathcal{E}}{\text{arg min}} [J_{ss}(\{j, l\})]$  ▷ Best 2-Target-cycle to cover
4:  $\Xi := \{j^*, l^*\}$ ,  $\xi := \{(j^*, l^*), (l^*, j^*)\}$  ▷ initial target-cycle
5: do ▷ Best way to expand  $\Xi$ 
6:    $[val, (i^*, (j^*, l^*)) := \underset{(j, l) \in \xi}{\text{arg max}}_{(i, (j, l)): i \in \mathcal{V} \setminus \Xi, [\Delta J_T(i | \xi, (j, l))]$  ▷ The edge to remove
7:   Replace  $(j^*, l^*) \in \xi$  with  $\{(j^*, i^*), (i^*, l^*)\}$  ▷ Updating  $\xi$ 
8:   Insert  $i^*$  into  $\Xi$  between  $j^*$  and  $l^*$ . ▷ Updating  $\Xi$ 
9: while  $val \geq 0$  ▷ Until marginal gain become negative
10:  $\Xi^\# := \Xi$ ;  $\xi^\# := \xi$ ; Return;
```

Algorithm 2 The algorithm used to generate the initial TCP $\Theta^{a(0)}$ from the obtained target-cycle Ξ^R, ξ^R .

```

1: Input: Graph  $\mathcal{G} = (\mathcal{V}, \mathcal{E})$ , and the target-cycle  $\Xi^R, \xi^R$ .
2: Output:  $\Theta^{a(0)}$  ▷ TCP values for agent  $a \in \mathcal{A}$ 
3:  $\Theta^1 := \mathbf{0} \in \mathbb{R}^{M \times M}$  ▷ Placeholders for  $\theta_{ij}^{a(0)}$  values
4: for  $i$  in  $\Xi^R$  do
5:   for  $j$  in  $\mathcal{V}$  do
6:     if  $i = j$  or  $(i, j) \in \xi^R$  then
7:        $\Theta^1[i][j] = 0$ ;
8:     else if  $(i, j) \in \mathcal{E}$  then
9:        $\Theta^1[i][j] = P$ ;
10:    else
11:       $\Theta^1[i][j] = \infty$ ;
12:    end if
13:  end for
14: end for
15:  $\Theta^{a(0)} := \Theta^1$ ; Return;
```

improved using the gradient steps (8). To ensure Ξ^R is a local optimal, after 100 iterations (at $l = 100$), the derived TCP $\Theta^{(l)}$ is randomly perturbed. Then it can be seen that $\Theta^{(l)}$ converges back to the same initial TCP found (with $J_T = 121.6$). It is important to note that this solution is better than the best TCP obtained with a random initialization of $\Theta^{(0)}$ (shown in Fig 3), by +7.6 (5.88%).

In order to highlight the importance of gradient steps, consider the new single-agent simulation example (SASE2) shown in Fig. 11. In there, when the TCP $\Theta^{(0)}$ is selected randomly, the gradient steps have converged to $J_T = 651.3$. Now, Fig. 12(a) shows the performance of the TCP given by the identified refined sub-optimal greedy cycle (obtained using Algorithm 1 and 2). As the usual next step, when gradient steps are used (8), compared to SASE1, we can now observe a further improvement in J_T (See Fig. 12(b) and (c)) which leads to a TCP Θ^* with $J_T = 567.0$. Therefore, the overall improvement achieved from deploying the proposing initialization technique is +84.3 (12.9%). The main difference between the solutions in Fig. 12(a) and (b) is that in the former one, agent avoids visiting the target 4 and strictly follows target-cycle shown in red color, whereas in the latter one, gradient descent steps have updated the TCP such that the agent trajectory now includes the target 4.

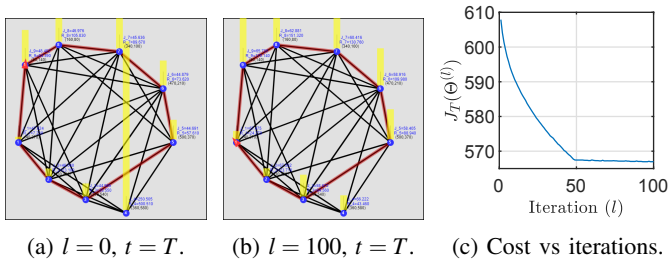


Fig. 12: SASE2: The TCP $\Theta^{(0)}$ given by the identified cycle Ξ^R (the red trace in (a),(b)) with cost $J_T = 607.9$ (improvement = +43.4 compared to Fig. 11) is further improved by the IPA based gradient updates (8). Final cost $J_T = 567.0$ (Improvement = +40.9 compared to (a)).

in Algorithm 1 when applied for the SASE1 problem configuration (first saw in Fig. 3). The target-cycle shown (as a red contour) in Fig. 13 (d) has a J_{ss} value of 135.7. A subsequently identified profitable refinement step and its final result is shown in Fig. 13 (e) and (f) respectively. The J_{ss} value of the target-cycle shown in Fig. 13 (f) is 128.7.

The identified target-cycle (say Ξ^R) is then converted to the respective TCP using Algorithm 2. Fig. 10(b) shows that the target-cycle Ξ^R has a J_T value of 121.6 which cannot be further

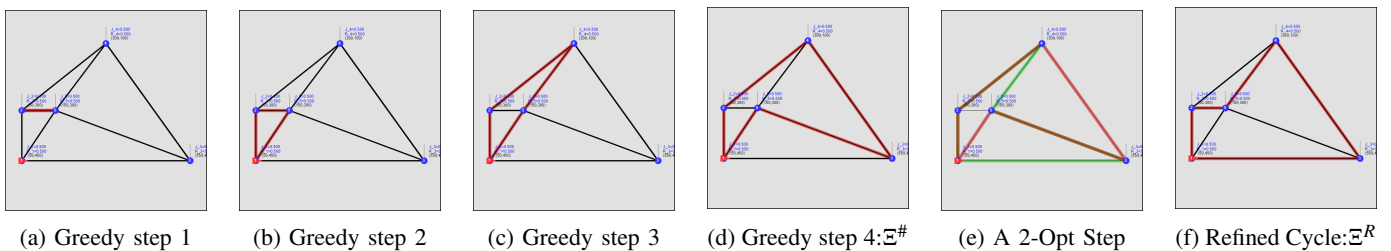


Fig. 13: Greedy target-cycle construction iterations (by Algorithm 1) and a profitable refinement step (a 2-Opt one) observed for the target topology of SASE1.

IV. CYCLIC PERSISTENT MONITORING ON SPARSE (GENERIC) GRAPHS WITH 1 AGENT

According to Assumption 1, the work presented so far assumes the underlying target topology to be bi-triangular (See Definition 1). Under a such setting, we have discussed on how to: (i) analyze, (ii) iteratively construct, (iii) refine, and, (iv) transform (to a set of TCP values), unconstrained target-cycles. However, if the target topology is sparse, the proposed sub-optimal target-cycle construction method can fail.

This failure (if occurred) originates from the step 6 of the Algorithm 1 - with brute force search operation failing due to having a null feasible search space. To illustrate this, consider the two half-constructed target-cycles shown in Fig. 14. At this stage, either of those cycles cannot be expanded as there are no new edges which we can add to the current cycle (i.e., to ξ) so that those new edges connects any one of the remaining neglected targets into the current cycle (See Fig. 7). Further, note that if the graphs shown in Fig. 14 respectively had the edges (4,2) and (4,5), this error does not occur. Hence the importance of having a bi-triangular graph for the execution of Algorithm 1 is clear.

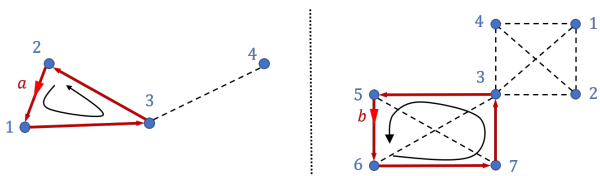


Fig. 14: Two example sparse graphs where Algorithm 1 has failed halfway through the cycle construction process.

A. The concept of ‘Auxiliary Targets’

In order to generalize the target-cycle construction procedure for sparse graph situations, we now propose to allow (some) targets to be visited more than once during a cycle. We call such target-cycles as *constrained target-cycles* - as oppose to the unconstrained target-cycles which we studied in the previous section. For an example, in both graphs shown in Fig. 14, if the target 3 is allowed to be visited more than once during a cycle, we could have formed the target-cycles $\Xi_a = \{2, 1, 3, 4, 3\}$ and $\Xi_b = \{6, 7, 3, 2, 1, 4, 3, 5\}$ respectively - so that no target is being neglected in each case. Note that in both Ξ_a and Ξ_b , there are two entries of target 3.

Giving this new flexibility (of allowing multiple visits to (some) targets during a cycle) ensures that we can form a

complete target-cycle without any target being neglected - irrespective of the sparseness of the given graph. However, this new flexibility raises a new set of challenges. Specifically, we now need find how to: (i) analyze, (ii) iteratively construct, (iii) refine, and, (iii) transform (to a set of TCP values), such constrained target-cycles.

To aid the process of addressing these challenges, we introduce a novel concept called *Auxiliary Targets* - which allows us to convert any constrained target-cycle into an **equivalent** unconstrained target-cycle. The purpose of this conversion is to use some of the already developed techniques initially utilized in analyzing unconstrained target-cycles.

Consider a constrained target-cycle Ξ with a target $i \in \Xi$ being visited n times during the cycle. Then, we first introduce an auxiliary target pool $\mathcal{T}_i = \{i^1, i^2, \dots, i^n\}$ where each auxiliary target i^j , $j \in \{1, 2, \dots, n\}$ can be thought of as a dummy/virtual target of the original target i , but, with its own set of parameters: uncertainty rate A_i^j and a sensing rate B_i^j . Note that, at this stage, we do not know the numerical values of auxiliary target parameters A_i^j or B_i^j , $\forall j \in \{1, 2, \dots, n\}$.

As the next step, each repeated element of target i found in Ξ is replaced with an element taken from \mathcal{T}_i respectively. Then, we repeat this process for all $i \in \Xi$ with more than one visit per cycle. Let’s denote the resulting unconstrained target-cycle as Ξ^u .

In order to illustrate this process, consider the constrained target-cycles Ξ_a and Ξ_b mentioned before regarding graphs in Fig. 14. Now, with the introduction of auxiliary targets for target 3 ($\mathcal{T}_3 = \{3^1, 3^2\}$), their unconstrained versions are $\Xi_a^u = \{2, 1, 3^1, 4, 3^2\}$ and $\Xi_b^u = \{6, 7, 3^1, 2, 1, 4, 3^2, 5\}$ respectively. These unconstrained target-cycles are illustrated in Fig. 15. Also, another example is shown in Fig. 16.

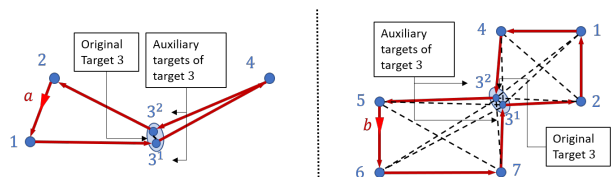


Fig. 15: Example 1: Converting constrained target-cycles into unconstrained target-cycles with the use of auxiliary targets.

Equivalence criteria: Once the unconstrained target-cycle Ξ^u corresponding to the interested constrained target-cycle Ξ is obtained, we next need to find the auxiliary target parameters of all the auxiliary targets present in Ξ^u . For this

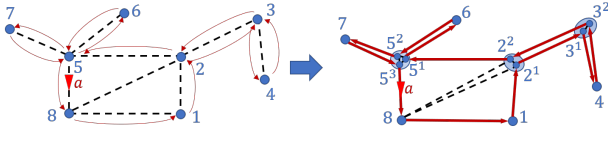


Fig. 16: Example 2: Converting constrained target-cycles into unconstrained target-cycles with the use of auxiliary targets.

purpose, we use the fact that both Ξ^u and Ξ perform/behave in an equivalent manner. Specifically, we enforce the following *equivalence criteria* between Ξ^u and Ξ .

- 1) For all targets $i^j \in \Xi^u$: The dwell time spent at the auxiliary target $i^j \in \Xi^u$ is **equal** to the dwell time spent at target $i \in \Xi$ on its j^{th} visit during a cycle.
- 2) For all targets $i^j \in \Xi^u$: The physical location of the auxiliary target i^j is same as the physical location of target i .
- 3) For all targets $i \in \Xi$: The overall contribution to the mean system uncertainty J_T by the auxiliary target pool \mathcal{T}_i of Ξ^u is **equal** to that of target $i \in \Xi$ during a cycle.

The first two conditions ensure that the time required to complete a cycle (for an agent) is the same for both Ξ^u and Ξ . If the numerical values of auxiliary target parameters are known, we can apply Theorem 1 to evaluate $J_{ss}(\Xi^u)$. And due to the third equivalence criteria, $J_{ss}(\Xi) = J_{ss}(\Xi^u)$. Therefore, it is clear how the concept of auxiliary targets can enable us evaluating the steady state mean cycle uncertainty value of Ξ .

Sub-cycle of an auxiliary target: Notice that each auxiliary target $i^j \in \Xi^u$ can be assigned with its own *sub-cycle* denoted by $\Xi_i^{u,j}$ such that the set $\{\Xi_i^{u,j} : i^j \in \mathcal{T}_i\}$ is a partition of the complete cycle Ξ^u around the target i . Specifically, each sub-cycle $\Xi_i^{u,j}$ starts with the immediate next target to $i^{j-1} \in \Xi^u$ and ends with target i^j . Therefore, Ξ^u can be written as a sum of sub-cycle partitions around the target i ,

$$\Xi^u = \bigcup_{j:i^j \in \mathcal{T}_i} \Xi_i^{u,j} \quad (28)$$

For example, on the unconstrained cycle shown in 16, the target 5 has three auxiliary targets $\mathcal{T}_5 = \{5^1, 5^2, 5^3\}$. Their respective sub-cycles would be: $\Xi_5^{u,1} = \Xi^u \setminus (\Xi_5^{u,2} \cup \Xi_5^{u,3})$, $\Xi_5^{u,2} = \{6, 5^2\}$, and, $\Xi_5^{u,3} = \{7, 5^3\}$. If a target $i \in \Xi^u$ does not have any auxiliary targets, then its sub-cycle (denoted as Ξ_i^u) would be $\Xi_i^u = \Xi^u$ (i.e., the complete unconstrained target-cycle).

The *sub-cycle unit vector* denoted by $\bar{\mathbf{I}}_{\Xi_i^{u,j}}$ is a $|\Xi^u|$ -dimensional column vector with ones located at sub-cycle $\Xi_i^{u,j}$'s target locations and zeros located at other locations. Analogous to (28), taking $\bar{\mathbf{I}}_{|\Xi^u|} \in \mathbb{R}^{|\Xi^u|}$ as a column vector of all ones, we can write (for a target i),

$$\bar{\mathbf{I}}_{|\Xi^u|} = \sum_{j:i^j \in \mathcal{T}_i} \bar{\mathbf{I}}_{\Xi_i^{u,j}} \quad (29)$$

Also, if a target $i \in \Xi^u$ does not have auxiliary targets, then its sub-cycle unit vector (denoted as $\bar{\mathbf{I}}_{\Xi_i^u}$) would be $\bar{\mathbf{I}}_{\Xi_i^u} = \bar{\mathbf{I}}_{|\Xi^u|}$.

The *sub-cycle matrix* of Ξ^u denoted by $\mathbf{1}_{\Xi^u}$ is a $|\Xi^u| \times |\Xi^u|$ matrix with each column being the respective target's sub-cycle unit vector. Fig. 17 shows an example sub-cycle matrix. Note that if the considered target-cycle Ξ is unconstrained, then $\mathbf{1}_{\Xi} \in \mathbb{R}^{|\Xi| \times |\Xi|}$ with all elements as 1 (i.e., $\mathbf{1}_{\Xi} = \bar{\mathbf{I}}_{|\Xi|} \bar{\mathbf{I}}_{|\Xi|}^T$).

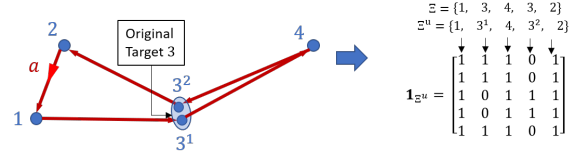


Fig. 17: Sub-cycle unit vectors and sub-cycle matrix (right) for a given constrained target-cycle Ξ .

B. Analysis of a constrained target-cycles

Let us consider the constrained target-cycle $\Xi = \{1, 2, \dots, n, n+1, \dots, n+m-1, n\}$ shown in Fig. 18 where the target n is visited twice during a cycle. As mentioned before, we introduce the auxiliary targets $\mathcal{T}_n = \{n^1, n^2\}$ to replace the target n entries in Ξ and get the unconstrained target-cycle Ξ^u of Ξ . The sub-cycles corresponding to the introduced auxiliary targets n^1 and n^2 would be $\Xi_n^{u,1} = \{1, 2, \dots, n-1, n^1\}$ and $\Xi_n^{u,2} = \{n+1, n+2, \dots, n+m-1, n^2\}$ respectively.

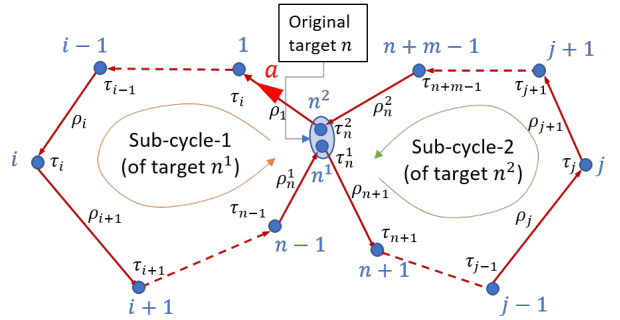


Fig. 18: A general constrained target-cycle with target n being visited twice during the cycle.

Regarding the agent behavior on the considered cycle Ξ , we use the same Assumption 2. A *tour* on Ξ starts/ends when the agent (a) leaves the target n to reach target 1. Note that the inter-target travel times have been labelled in a similar manner to that of Fig. 5, except for the entries ρ_n^1 and ρ_n^2 which denotes the time to reach target n on each visit to it - from the previous targets on Ξ , target $(n-1)$ and target $(n+m-1)$ respectively. We use the notation $\bar{\rho}_{\Xi^u} = [\rho_1, \rho_2, \dots, \rho_{n-1}, \rho_n^1, \rho_n^2, \rho_{n+1}, \dots, \rho_{n+m-1}, \rho_n^2]^T$ as the *travel time vector* of the cycle Ξ^u .

To simplify the analysis, we will not focus on the transient behavior of the considered cycle Ξ , unlike what we did in the previous section. This means we will not be analyzing how the agent dwell times (at different targets in Ξ) evolved over the number of tours made on Ξ (like in (13)). Therefore, we need to make the following assumption.

Assumption 5. *The dwell time dynamics of the constrained target-cycle Ξ (shown in Fig. 18) has a feasible equilibrium point which is globally asymptotically stable.*

When the dwell time dynamics have converged to the equilibrium point as per the Assumption 5, the overall system is said to be operating in its steady state. Fig. 19 shows such a steady state behavior of target uncertainties during a tour on the cycle Ξ . The notation $\bar{\tau}_{\Xi^u} = [\tau_1, \tau_2, \dots, \tau_n^1, \dots, \tau_{n+m-1}, \tau_n^2]^T$

is used to represent the steady state dwell times on the cycle Ξ^u . Following lemma is proposed to evaluate $\bar{\tau}_{\Xi^u}$ value for a given target-cycle Ξ (applicable to both constrained or unconstrained target-cycles).

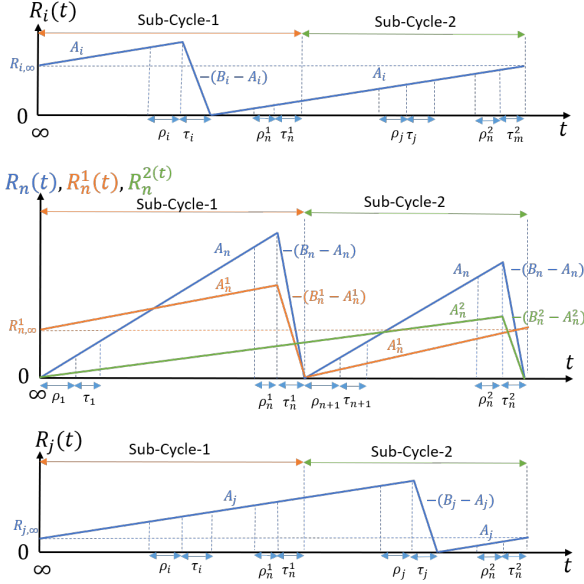


Fig. 19: Variation of target uncertainties of the constrained target-cycle shown in Fig. 18 - after achieving the steady state.

Lemma 5. Under Assumption 2 and 5, when a single agent traverses on a generic target-cycle Ξ (with Ξ^u being the converted version with auxiliary targets), the steady state dwell times $\bar{\tau}_{\Xi^u}$ are given by,

$$\bar{\tau}_{\Xi^u} = [\text{diag}(\bar{\gamma}_{\Xi}) - \mathbf{1}_{\Xi^u}]^{-1} \mathbf{1}_{\Xi^u} \bar{\rho}_{\Xi^u}, \quad (30)$$

where, if the i^{th} target of Ξ is j , then, i^{th} element of $\bar{\gamma}_{\Xi} \in \mathbb{R}^{|\Xi|}$ is $\frac{B_j}{A_j}$. And $\mathbf{1}_{\Xi^u}$ is the sub-cycle matrix and $\bar{\rho}_{\Xi^u}$ is the travel time matrix of the target-cycle Ξ^u .

Proof. From $R_n(t)$ profile in Fig. 19, it is clear that for each auxiliary target of the target n , when the corresponding sub-cycle period is considered, we can write,

$$B_n \tau_n^j = A_n T_{\Xi^u, j} \quad \forall j \ni n^j \in \mathcal{T}_n. \quad (31)$$

where, $T_{\Xi^u, j}$ is the total time taken to complete the sub-cycle of the target n^j . Further, note that the above equation is applicable for any target on the cycle Ξ^u (due to the flexibility of the definition of a sub-cycle). Furthermore, this relationship is generally applicable for any arbitrary target-cycle Ξ . Now, with the use of sub-cycle unit vectors, we can substitute for $T_{\Xi^u, j}$ to get, for all $n \in \Xi$,

$$B_n \tau_n^j = A_n \bar{\mathbf{1}}_{\Xi^u, j}^T (\bar{\rho}_{\Xi^u} + \bar{\tau}_{\Xi^u}), \quad \forall j \ni n^j \in \mathcal{T}_n, \quad (32)$$

This gives us with $|\Xi^u|$ number of equations. We need to solve for $\bar{\tau}_{\Xi^u} \in \mathbb{R}^{|\Xi^u|}$. This can be achieved arranging all the equations in a matrix form,

$$\begin{aligned} \text{diag}(\bar{\gamma}_{\Xi}) \bar{\tau}_{\Xi^u} &= \mathbf{1}_{\Xi^u} (\bar{\rho}_{\Xi^u} + \bar{\tau}_{\Xi^u}), \\ \therefore \bar{\tau}_{\Xi^u} &= [\text{diag}(\bar{\gamma}_{\Xi}) - \mathbf{1}_{\Xi^u}]^{-1} \mathbf{1}_{\Xi^u} \bar{\rho}_{\Xi^u}. \end{aligned} \quad (33)$$

It is important to note that Lemma 5 is applicable to any general target-cycle Ξ . Hence when the interested target-cycle Ξ is an unconstrained one, it is easy to show that both steady state dwell time values given by Lemma 5 and Lemma 2 are identical. \square

Remark 1. From Lemma 5 we can comment on the the dwell time dynamics of constrained target-cycles: The condition for the existence of an equilibrium point is: $|\text{diag}(\bar{\gamma}_{\Xi}) - \mathbf{1}_{\Xi^u}| \neq 0$ and the feasibility condition is $\bar{\tau}_{\Xi^u} > 0$.

Remark 2. Unlike what we did in Lemma 2, here (in Lemma 5) we cannot use Lemma 1 to further simplify the inverse: $[\text{diag}(\bar{\gamma}_{\Xi}) - \mathbf{1}_{\Xi^u}]^{-1}$. However, we can show that $\text{rank}(\mathbf{1}_{\Xi^u}) = (\text{number of auxiliary targets in } \Xi^u) \ll |\Xi^u|$. Therefore, kenmiller theorem proposed in [22] (which is an improved version of Lemma 1) can be used to efficiently compute $[\text{diag}(\bar{\gamma}_{\Xi}) - \mathbf{1}_{\Xi^u}]^{-1}$.

Using Lemma 5, we can find the dwell time vector $\bar{\tau}_{\Xi^u}$. Further, we already know the travel times vector $\bar{\rho}_{\Xi^u}$. Therefore, we now can find the total sub-cycle times denoted by $T_{\Xi^u, j}$ for all targets $n^j \in \Xi^u$, as,

$$T_{\Xi^u, j} = \bar{\mathbf{1}}_{\Xi^u, j}^T (\bar{\rho}_{\Xi^u} + \bar{\tau}_{\Xi^u}). \quad (34)$$

Furthermore, when the total sub-cycle time metric evaluated for an actual target (which does not have any auxiliary targets), we get the total cycle time value denoted by T_{Ξ^u} where,

$$T_{\Xi^u} = \bar{\mathbf{1}}_{|\Xi|}^T (\bar{\rho}_{\Xi^u} + \bar{\tau}_{\Xi^u}). \quad (35)$$

Lemma 6. Under the same conditions stated in Lemma 5, the auxiliary target parameters of an auxiliary target $n^j \in \Xi^u$ (i.e., A_n^j and B_n^j) are, (valid $\forall j \ni n^j \in \mathcal{T}_n, \forall n \in \Xi$.)

$$\begin{aligned} A_n^j &= \frac{T_{\Xi^u, j} \tau_n^j (B_n - A_n)}{T_{\Xi^u} (T_{\Xi^u} - \tau_n^j)}, \text{ and,} \\ B_n^j &= \frac{T_{\Xi^u, j} (B_n - A_n)}{(T_{\Xi^u} - \tau_n^j)}. \end{aligned} \quad (36)$$

Proof. Note the auxiliary target uncertainty profiles $R_n^1(t), R_n^2(t)$ drawn in Fig. 19 for the target-cycle shown in Fig. 18. The shape of these profiles should satisfy the equivalence criteria we established.

Using these graphs, for the complete cycle duration T_{Ξ^u} , we can write $B_n^j \tau_n^j = A_n^j T_{\Xi^u, j}$ for $j = 1, 2$. This result can be generalized to any generic target-cycle Ξ^u as,

$$B_n^j \tau_n^j = A_n^j T_{\Xi^u, j}, \quad \forall j \ni n^j \in \mathcal{T}_n, \forall n \in \Xi. \quad (37)$$

The above relationship ensures the first condition in the equivalence criteria.

Now, going back to the case of target-cycle shown in Fig. (18), to ensure the third condition in the equivalence criteria, we need:

$$\begin{aligned} \frac{1}{T_{\Xi^u}} \int_{T_{\Xi^u}} R_n^1(t) dt + \frac{1}{T_{\Xi^u}} \int_{T_{\Xi^u}} R_n^2(t) dt &= \frac{1}{T_{\Xi^u}} \int_{T_{\Xi^u}} R_n(t) dt \\ &= \frac{1}{T_{\Xi^u}} \int_{T_{\Xi^u, 1}} R_n(t) dt + \frac{1}{T_{\Xi^u}} \int_{T_{\Xi^u, 2}} R_n(t) dt \end{aligned} \quad (38)$$

Here, we can get two equations by equating individual terms in L.H.S. and R.H.S. This result can be generalized to any generic target-cycle Ξ^u as,

$$\int_{T_{\Xi^u}} R_n^j(t) dt = \int_{T_{\Xi^u, j}} R_n(t) dt, \quad \forall j \ni n^j \in \mathcal{T}_n, \quad \forall n \in \Xi. \quad (39)$$

Since the uncertainty profiles are piece-wise linear, we can evaluate the integrals above and get the required condition as,

$$(B_n^j - A_n^j) = \frac{T_{\Xi^u, j}}{T_{\Xi^u}} (B_n - A_n) \quad \forall j \ni n^j \in \mathcal{T}_n, \quad \forall n \in \Xi. \quad (40)$$

Finally, we can solve (37) and (40) to obtain the numerical values of auxiliary target parameters: $\{(A_n^j, B_n^j) : \forall j \ni n^j \in \mathcal{T}_n, \forall n \in \Xi\}$. \square

Using Lemma 6, we can find all the unknown target uncertainty and sensing rate parameters of the targets listed in Ξ^u . Now, Let us lump those parameters in vectors \bar{A}_{Ξ^u} and \bar{B}_{Ξ^u} respectively. For example, for the target-cycle shown in Fig. 18, $\bar{A}_{\Xi^u} = [A_1, A_2, \dots, A_n^1, \dots, A_{n+m-1}, A_n^2]^T$. With this notation, we can propose our main theorem as follows.

Theorem 3. *Under Assumption 2 and 5, when a single agent traverses on a generic target-cycle Ξ (with Ξ^u being the converted version of it with auxiliary targets), the steady state mean cycle uncertainty $J_{ss}(\Xi)$ is given by,*

$$J_{ss}(\Xi) = \frac{1}{2} (\bar{B}_{\Xi^u} - \bar{A}_{\Xi^u})^T \bar{\tau}_{\Xi^u}, \quad (41)$$

where, $\bar{\tau}_{\Xi^u}$ is given by Lemma 5 and unknown elements of $\bar{A}_{\Xi^u}, \bar{B}_{\Xi^u}$ (i.e., the auxiliary target parameters) are computed using Lemma 6.

Proof. Note that the converted target-cycle Ξ^u obtained from any given general target-cycle Ξ , will be an unconstrained target-cycle. Therefore, we can use Theorem 1 and write,

$$J_{ss}(\Xi^u) = \frac{1}{2} (\bar{B}_{\Xi^u} - \bar{A}_{\Xi^u})^T \bar{\tau}_{\Xi^u}. \quad (42)$$

To evaluate this, we need to first compute $\bar{\tau}_{\Xi^u}$ using Lemma 5. Then, any unknown parameters remaining on the vectors \bar{A}_{Ξ^u} and \bar{B}_{Ξ^u} should be computed using Lemma 6 (or by just using (40)). Finally, according to equivalence criteria condition 3 we get $J_{ss}(\Xi) = J_{ss}(\Xi^u)$. \square

C. Sub-optimal target-cycle construction via a greedy scheme

For single agent persistent monitoring problems on a target topology \mathcal{G} , if the set $\mathcal{D} = \{\text{All possible target-cycles on } \mathcal{G}\}$ has a low cardinality, then we can find the best performing target-cycle (at steady state) given by,

$$\Xi^* = \arg \min_{\Xi \in \mathcal{D}} J_{ss}(\Xi) \quad (43)$$

using Theorem 3 via a brute force search. Since $\mathcal{C} \subseteq \mathcal{D}$, compared to (24), the solution to (43) will have a lower (better) cost. However, since the size of the search space $|\mathcal{D}|$ grows exponentially with $|\mathcal{V}|$, we seek to construct a greedy scheme which can provide an approximate solution to (43).

Target-cycle expansion operation - Type 1 (TCEO-1):

Note that the greedy scheme given in Algorithm 1 iteratively uses a target-cycle expansion operation (TCEO) (shown in Fig. 7, and also in Fig. 20 (a) \rightarrow (b)) to construct a sub-optimal unconstrained target-cycle for (24). Let us label this type of a TCEO as a TCEO-1. The gain in the objective function due to a TCEO-1 is given in Theorem 2 as a function $\Delta J_T(i|\xi, (j, l))$ (from now onward, we denote this by $\Delta J_T^1(i|\xi, (j, l))$). Also, when started with an unconstrained target-cycle, the TCEO-1 will always result an unconstrained target-cycle. However, in (43), the search space \mathcal{D} contains both unconstrained and constrained target-cycles. Therefore, new TCEOs should be introduced (apart from the TCEO-1).

Target-cycle expansion operation - Type 2 (TCEO-2):

Consider a generic target-cycle Ξ (with its list of edges being ξ and their respective converted versions being Ξ^u and ξ^u). In TCEO-2, connecting an external target $i \in \mathcal{V} \setminus \Xi$ to the Ξ is done via creating an additional auxiliary target to one of the targets $j \in \Xi$ when $(j, i) \in \mathcal{E}$. Specifically, if this expansion happens at target $j^k \in \Xi^u$, then, to get the expanded cycle Ξ^u (and ξ^u), (i) all the auxiliary targets $j^l \in \Xi^u, l > k$ should be relabelled to j^{l+1} in both Ξ^u and ξ^u , (ii) two new targets i and j^{k+1} should be inserted after the target j^k in Ξ^u , (iii) two new edges (j^k, i) and (i, j^{k+1}) should be inserted after the edge (\cdot, j^k) in ξ^u .

The result of a TCEO-2 (say Ξ') will always be a constrained target-cycle. A marginal gain function of the form $\Delta J_T^2(i|\Xi^u, j^k)$ can be proposed to evaluate the gain of a such TCEO-2 step as, (similar to Theorem 2)

$$\Delta J_T^2(i|\Xi^u, j^k) = \left(R_{i,0} + \frac{A_i T}{2} \right) + J_{ss}(\Xi) - J_{ss}(\Xi'). \quad (44)$$

An example of this TCEO-2 is shown in Fig. 20 (a) \rightarrow (c) where an additional auxiliary target (3^3) has been created to expand the current target-cycle so that it includes the external target i .

Take $\|\Xi\|$ as the number of distinguishable entries in the set Ξ . It is important to note that when the graph \mathcal{G} is *connected*, and the target-cycle Ξ is such that $\|\Xi\| < |\mathcal{V}|$, we can always increase $\|\Xi\|$ using TCEO-2 on Ξ . Also note that when $\|\Xi\| = |\mathcal{V}|$, the target-cycle goes through all the targets in the given graph. Therefore, this property of TCEO-2 is useful in constructing an improved greedy scheme which can overcome the situations like the ones shown in Fig. 14 (where Algorithm 1 fails).

Target-cycle expansion operation - Type 3 (TCEO-3):

Let us consider a situation where we have a generic target-cycle Ξ . We use the notation $[j^k, l^m]$ to represent the ordered set of targets in Ξ^u that are exclusively in-between the two non-adjacent targets $j^k \in \Xi^u$ and $l^m \in \Xi^u$. If: (i) an external target i has feasible edges to targets $j^k, l^m \in \Xi^u$ (i.e., $(j^k, i), (i, l^m) \in \mathcal{E}$) and, (ii) all the targets in $[j^k, l^m]$ have other auxiliary targets (i.e., $[j^k, l^m] \subseteq \text{Aux} = \Xi^u \setminus \Xi$), then, we can perform the TCEO-3. Specifically, in TCEO-3, following operations are carried out: (i) The set of targets $[j^k, l^m]$ in Ξ^u are replaced with i , (ii) The respective edges in ξ^u are replaced with two edges $(j^k, i), (i, l^m)$, and, (iii) All the auxiliary targets of the targets in $[j^k, l^m]$ are relabelled.

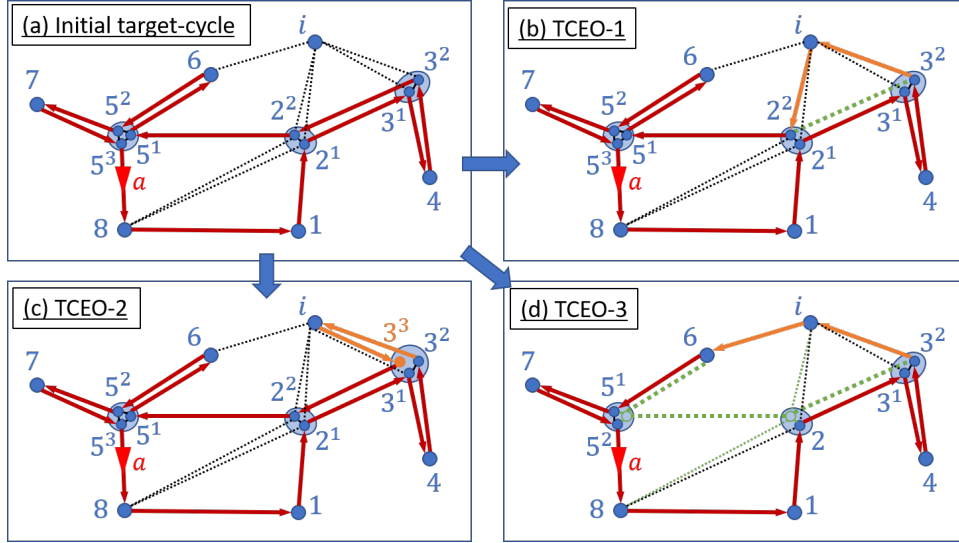


Fig. 20: Target-cycle expansion operations.

Note that, to perform TCEO-3, Ξ should be a constrained target-cycle. However, the resulting expanded target-cycle (say Ξ') is not necessarily a constrained target-cycle, as TCEO-3 always cancels out a set of auxiliary targets (specifically the set $[j^k, l^m]$). Similar to (27) and (44), following the Theorem 2, a marginal gain function $\Delta J_T^3(i|\Xi^u, [j^k, l^m])$ where,

$$\Delta J_T^3(i|\Xi^u, [j^k, l^m]) = \left(R_{i,0} + \frac{A_i T}{2} \right) + J_{ss}(\Xi) - J_{ss}(\Xi'), \quad (45)$$

can be used to represent the gain in the objective function due to the aforementioned generic TCEO-3.

An example of this TCEO-3 is shown in Fig. 20 (a) \rightarrow (d), where the set of auxiliary targets $[3^2, 6] = \{2^2, 5^1\}$ are cancelled out with the insertion of the external target i in the expanded target-cycle.

Improved Greedy algorithm: Now, we propose the improved greedy scheme which can construct a sub-optimal target-cycle for the problem in (43) given the target topology. Unlike in Algorithm 1, in this improved greedy scheme (given below in Algorithm 3), the search space of each iteration is not limited to unconstrained target-cycles. Therefore, this improved greedy scheme will work even under sparse graph conditions.

It starts from searching for the best target-cycle of length 2 (i.e. $\Xi \ni |\Xi| = 2$) and the obtained solution is then used as the initial target-cycle. Next, the current target-cycle is expanded by adding an external target in each iteration. The steps 6,7 and 8 searches for the best method of expanding the current target-cycle under TCEO-1, TCEO-2, and TCEO-3, respectively. In step 8, the set variable $Aux = \Xi^u \setminus \Xi$ represents the set of all introduced auxiliary targets. Then, steps 9-15 aims to execute the TCEO with the highest marginal gain.

Refining the obtained generic target-cycle: If the sub-optimal target-cycle given by the greedy Algorithm 3 (say $\Xi^\#$) is an unconstrained one, we can apply the previously discussed TSP inspired 2-Opt and 3-Opt techniques (see Fig. 8) to further improve (refine) the obtained solution $\Xi^\#$. However, when $\Xi^\#$

is a constrained target-cycle, applicability of such 2-Opt or 3-Opt techniques is not straight forward - because some targets are being visited more than once during the target-cycle $\Xi^\#$ (contrary to the TSP problem scenarios).

To overcome this challenge, we execute the following set of steps:

- 1) Execute a 2-Opt (or a 3-Opt) operation on the converted version of $\Xi^\#$ (i.e., on $\Xi^{\#u}$ assuming all the auxiliary targets in a set \mathcal{T}_i are fully connected (with zero distance links) for all targets $i \in \Xi^\#$. Take the resulting target-cycle as Ξ^1 .
- 2) If Ξ^1 utilizes one of the aforementioned zero distance links (say the link between (i^j, i^k)), it means we can now merge the two auxiliary targets (i^j, i^k) into a single auxiliary target i^l (where $l = \min(j, k)$). Take the resulting target-cycle as Ξ^2 .
- 3) (Inspired by the TCEO-3) If there exists two distinct non-adjacent targets $j^k, l^m \in \Xi^{2u}$ such that (i) $(j^k, l^m) \in \mathcal{E}$, and (ii) $[j^k, l^m] \subseteq Aux = \Xi^{2u} \setminus \Xi^2$, then, we can (i) remove all the auxiliary targets $[j^k, l^m]$ from Ξ^{2u} , and, (ii) replace the respective edges in Ξ^{2u} with just the edge (j^k, l^m) . Take resulting target-cycle as Ξ^3 .
- 4) Now, if $J_{ss}(\Xi^3) \leq J_{ss}(\Xi^\#)$ update $\Xi^\# := \Xi^3$ and continue to step (1) above.

As an example, see the process shown in Fig. 21 (a) \rightarrow (b) \rightarrow (c) \rightarrow (d). It is a case where a 2-Opt operation has been carried out with a consequent auxiliary target merging step (i.e., refinement step (1) and (2) given above) - to generate a new perturbed target-cycle. Also, the direct step Fig. 21 (a) \rightarrow (d) can be seen as an example for the refinement step (3) given above - where the auxiliary target set $[4, 2] = \{3^2\}$ is being removed due to the existence of the direct link $(4, 2) \in \mathcal{E}$.

Once each of the possible 2-Opt and 3-Opt operations for the current target-cycle $\Xi^\#$ have been evaluated according to the above set of steps, and when none of those resulting target-cycles (i.e., Ξ^3 cycles) has a lower value than $J_{ss}(\Xi^\#)$, then, we call the target-cycle $\Xi^\#$ as the refined sub-optimal target-cycle

Algorithm 3 The proposing improved greedy algorithm for sub-optimal target-cycle construction under assumptions 2 and 4 with a single agent.

1: **Input:** Target topology $\mathcal{G} = (\mathcal{V}, \mathcal{E})$, where, $\mathcal{V} = \{1, 2, \dots, M\}$, and, $\mathcal{E} = \{(i, j) : i, j \in \mathcal{V}, \text{Edge } (i, j) \text{ available to travel}\}$.

2: **Output:** A sub-optimal target-cycle $\Xi^\#$ (and $\xi^\#$).

3: $(j^*, l^*) := \arg \min_{(j, l) \in \mathcal{E}} J_{ss}(\{j, l\})$ ▷ Identifying the best 2-Target-cycle to cover

4: $\Xi := \{j^*, l^*\}$, $\xi := \{(j^*, l^*), (l^*, j^*)\}$ ▷ Initial target-cycle

5: **do**

6: $[val_1, (i^*, (j^*, l^*))_1] := \underset{\substack{(i, (j, l)): i \in \mathcal{V} \setminus \Xi, \\ (j, l) \in \xi}}{\arg \max} [\Delta J_T^1(i | \xi^u, (j, l))]_1$ ▷ Identifying the best available TCEO-1

7: $[val_2, (i^*, j^{k*})_2] := \underset{\substack{(i, j^k): i \in \mathcal{V} \setminus \Xi, \\ j^k \in \Xi^u}}{\arg \max} [\Delta J_T^2(i | \Xi^u, j^k)]_2$ ▷ Identifying the best available TCEO-2

8: $[val_3, (i^*, [j^{k*}, l^{m*}]_3] := \underset{\substack{(i, j^k, l^m): i \in \mathcal{V} \setminus \Xi, \\ j^k, l^m \in \Xi^u, \\ [j^k, l^m] \subseteq Aux}}{\arg \max} [\Delta J_T^3(i | \Xi^u, [j^k, l^m])]_3$ ▷ Identifying the best available TCEO-3

9: **if** $(val_1 \geq val_2)$ and $(val_1 \geq val_3)$ and $(val_1 > 0)$ **then** ▷ The found TCEO-1 is the most profitable!

10: **Execute** TCEO-1 on Ξ using $(i^*, (j^*, l^*))_1$

11: **else if** $(val_2 \geq val_3)$ and $(val_2 > 0)$ **then** ▷ The found TCEO-2 is the most profitable!

12: **Execute** TCEO-2 on Ξ using $(i^*, j^{k*})_2$

13: **else if** $(val_3 > 0)$ **then** ▷ The found TCEO-3 is the most profitable!

14: **Execute** TCEO-3 on Ξ using $(i^*, [j^{k*}, l^{m*}]_3$

15: **else**

16: **Break** ▷ No TCEO was found with a positive marginal gain.

17: **end if**

18: **while True**

19: $\Xi^\# := \Xi$; $\xi^\# := \xi$; **Return**;

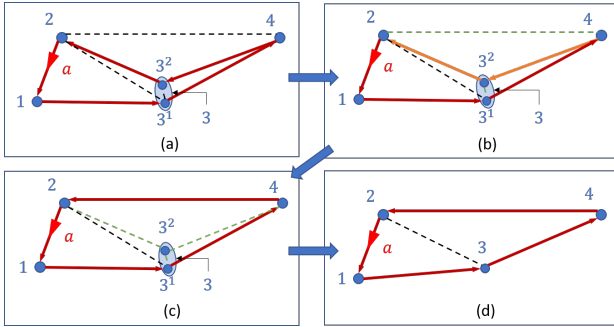


Fig. 21: Refinement steps on a constrained target-cycle.

and we represent it using the symbol Ξ^R .

D. The initial set of threshold control policy values: $\Theta^{(0)}$

As we did in the previous section, our final goal is to convert the refined sub-optimal target-cycle Ξ^R into a set of threshold control policy values: $\Theta^{(0)}$ so that it can be used in (8). Since we still consider only the single agent situations, $\mathcal{A} = \{a\}$, therefore, $\Theta^{(0)} = \Theta^{a(0)}$. Even though now Ξ^R can be a constrained target-cycle (as opposed to Ξ^R being a simple unconstrained target-cycle as before), we can still use the Algorithm 2 to get the corresponding $\Theta^{a(0)}$.

Notice that, now, if a target $i \in \Xi^R$ has n auxiliary targets (i.e., when $|\mathcal{T}_i| = n$) then, $(n+1)$ elements of the i^{th} row of $\Theta^{a(0)}$ will be 0. This is because, from the target i , an agent now have to have the ability to go to destinations $j \in \{\Xi_i^{Ru,k}[1] :$

$k \ni i^k \in \mathcal{T}_i\}$ (recall that $\Xi_i^{Ru,k}$ represents the sub-cycle of the auxiliary target $i^k \in \Xi^{Ru}$).

On the other hand, this means, when the agent is at target i , the target prioritization operation done in step 1 of (4) will now compare n distinct destination target uncertainties and pick the target with the maximum uncertainty as the next destination. An example (constrained) target-cycle and the respecting $\Theta^{a(0)}$ obtained from using Algorithm 2 is given in Fig. 22.

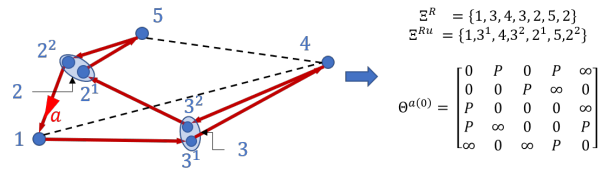


Fig. 22: The generated threshold matrix $\Theta^{a(0)}$ for the refined sub-optimal target-cycle Ξ^R shown (left).

However, it should be noted that the aforementioned scheme to get $\Theta^{a(0)}$ (i.e. using the Algorithm 2) will only work when for any target $i \in \Xi^R$, the uncertainty rates of the immediate destinations (i.e., $\{A_j : j \ni j \in \{\Xi_i^{Ru,k}[1] : k \ni i^k \in \mathcal{T}_i\}\}$) are not drastically different from each other.

Even if it is the case, it can be shown that when target $j_k = \Xi_i^{Ru,k}[1]$, $k \ni i^k \in \mathcal{T}_i$ is used to denote immediate neighbors of target i on the target-cycle Ξ^R , selecting thresholds such that,

$$\Theta^{a(0)}[i][j_k] = \theta_{i j_k}^{1(0)} = A_{j_k}(T_{\Xi^R} - \tau_{j_k} - t_{j_k} - \frac{1}{2} T_{\Xi_i^{Ru,k-1}}) \quad (46)$$

resolves this issue. Then, (46) can be used in step 7 of Algorithm 2 as opposed to setting $\theta_{i,jk}^{1(0)} = 0, \forall k \ni i^k \in \mathcal{T}_i$ and $\forall i \in \Xi^R$. (Recall the notation: T_{Ξ} is the total time spent on a target-cycle Ξ , τ_i is the steady state dwell time at a target i , and, t_i is the time to reach target i from the previous target on the considered target-cycle).

E. Simulation results

Fig. 23 (a)→(d) shows the intermediate cycles generated by the greedy sub-optimal cycle construction process given in Algorithm 3 when applied for the SASE1 problem configuration (See Fig. 3, 13 and 10). The target-cycle shown (as a red contour) in Fig. 23 (d) is $\Xi = \{2, 1, 2, 5, 3, 4, 5\}$ and it has a J_{ss} value of 121.1. Note that $J_{ss}(\Xi)$ is better than the J_{ss} value of the unconstrained target-cycle identified before (in Fig. 13(f)) by +7.6 (5.9%). This improvement is a result of the increased greedy search space size in Algorithm 3 w.r.t. Algorithm 1. Also note that in Ξ , both target 2 and target 5 are being visited twice per each cycle.

The identified target-cycle Ξ is then converted to the respective TCP using Algorithm 2. Fig. 24(b) shows that the target-cycle Ξ has a J_T value of 114.9 which cannot be further improved using the gradient steps (8). To ensure Ξ is a local optimal, after 100 iterations (at $l = 100$), the derived TCP $\Theta^{(0)}$ is randomly perturbed. Then it can be seen that $\Theta^{(l)}$ converges back to the same initial TCP found (with $J_T = 114.6$). It is important to note that this solution is better than the best TCP obtained with a random initialization of $\Theta^{(0)}$ (shown in Fig 3), by +13.8 (10.7%). And when compared to the unconstrained target cycle based solution shown in Fig. 10, it is an improvement of +6.7 (5.0%).

In order to illustrate the importance of gradient ascent steps, consider the new single agent simulation example (SASE3) shown in Fig. 25. When the TCP $\Theta^{(0)}$ is selected randomly, the gradient steps have converged to $J_T = 497.9$. Now, Fig. 26(a) shows the performance of the TCP given by the identified refined sub-optimal greedy constrained cycle (obtained using Algorithm 3 and 2). As the usual next step, when gradient steps are used (8), compared to SASE1, we can now observe a further improvement in J_T (See Fig. 26(b) and (c)) which leads to a TCP Θ^* with $J_T = 449.5$. Therefore, the overall improvement achieved from deploying the proposing initialization technique is +48.4 (9.7%).

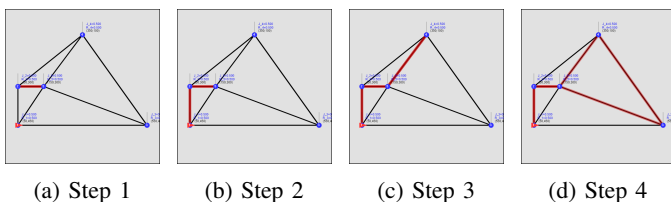


Fig. 23: Greedy target-cycle construction iterations (by Algorithm 3) observed for the target topology of SASE1.

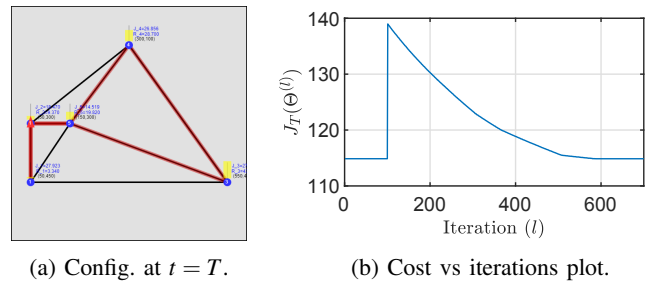


Fig. 24: SASE1: The TCP $\Theta^{(0)}$ given by the identified cycle Ξ^R (the red trace in (a)) shows local optimality. At $l = 100$, $\Theta^{(l)}$ is randomly perturbed. Yet, converges back to the initial TCP. Cost $J_T = 114.9$ (Improvement = +6.7 compared to Fig. 10).

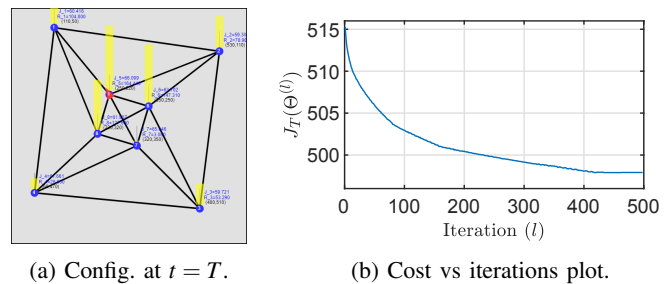


Fig. 25: Single agent simulation example 3 (SASE3): Starting with a random $\Theta^{(0)}$, converged to a TCP with the cost $J_T = 497.9$.

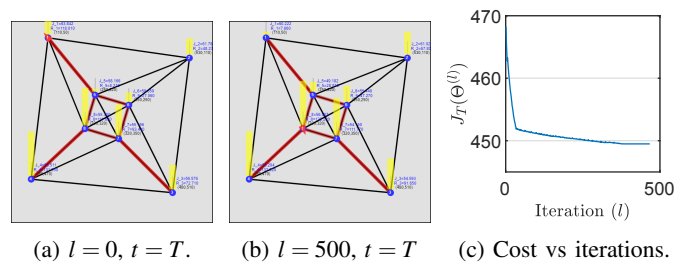


Fig. 26: SASE3: The TCP $\Theta^{(0)}$ given by the identified cycle Ξ^R (the red trace in (a),(b)) with cost $J_T = 468.2$ (improvement = +29.7 compared to Fig. 25) is further improved by the IPA based gradient updates (8). Final cost $J_T = 449.5$ (Improvement = +18.7 compared to (a)).

V. CYCLIC PERSISTENT MONITORING ON GENERIC GRAPHS WITH MULTIPLE AGENTS

The work presented so far considers only single agent persistent monitoring problems. Now, to extend the developed solution framework into multi-agent persistent monitoring problems, we propose to follow an approach where we first partition the considered graph topology \mathcal{G} into N sub-graphs, and then, allocate each agent $a \in \mathcal{A}$ into different sub-graphs.

Such partition-and-allocate (divide-and-conquer/non-cooperative) based approach was motivated due to three reasons: (i) The experimental results of the work in [15] suggests that in most graph structures, lower (better) objective function values (i.e., J_T in (2)) are attainable when agents do

not share targets in their steady state behavior, (ii) Extending the developed framework (in previous two sections) would be straightforward as once the graph \mathcal{G} is partitioned, it can be thought of as solving a set of independent single agent persistent monitoring problems (with each problem on a separate sub-graph), (iii) Since the overall goal of this work is to find a better initial condition $\Theta^{(0)}$ for the IPA based gradient descent steps in (8), we can expect the consequent $\Theta^{(l)}$ updates in (8) to break the non-cooperative nature of the initial solution $\Theta^{(0)}$ that we propose - if it is not optimal.

A. Overview of the complete solution

The steps of the complete solution that we propose for the problem of multi-agent persistent monitoring on graphs introduced in section II are outlined in the following algorithm.

Algorithm 4 The steps of the proposing complete solution to the problem of persistent monitoring on graphs.

1: Input:

- 1) Target topology $\mathcal{G} = (\mathcal{V}, \mathcal{E})$, with $\mathcal{V} = \{1, 2, \dots, M\}$ and $\mathcal{E} = \{(i, j) : i, j \in \mathcal{V}, \text{Edge } (i, j) \text{ available to travel}\}$,
- 2) Set of agents $\mathcal{A} = \{1, 2, \dots, N\}$,
- 3) Initial target uncertainties $\{R_i(0) : i \in \mathcal{V}\}$,
- 4) Initial agent locations $\{s_a(0) : a \in \mathcal{A}\}$,
- 5) Finite Time horizon T .

2: Output: A locally optimal threshold based control policy values: Θ^*

- 3: Partition the given graph \mathcal{G} into N sub-graphs $\{\mathcal{G}_a\}_{a \in \mathcal{A}}$.
- 4: For each sub-graph \mathcal{G}_a , find the refined target-cycle Ξ^{Ra} .
- 5: Execute iterative refinements to the graph-partitioning.
- 6: Re-assign agents to cycles based on the shortest distance from initial agent location to the cycles.
- 7: Get threshold policies $\Theta^{a(0)}$ of cycles Ξ^{Ra} , $\forall a \in \mathcal{A}$.
- 8: Use $\Theta^{(0)}$ in (8) and update $\Theta^{(l)}$ using IPA gradients [15].

In the Algorithm 4, to execute the steps 4 and 7, we directly utilize the single-agent persistent monitoring techniques discussed in section IV. The final step (i.e., step 8) is executed according to [15] and was discussed in section II. The three remaining steps (i.e., step 3, 5 and 6) involve: (i) partitioning the graph, (ii) refining the decided graph partitions, and, (iii) assigning agents to the graph partitions (i.e., to the cycles on the graph partitions). These three topics will be discussed respectively in the following subsections.

B. Spectral clustering based graph partitioning

Introduction: In order to partition the given target topology \mathcal{G} , we use the *spectral clustering* [26] technique which is a commonly used global graph partitioning method. Compared to the traditional clustering techniques such as the k-means method, the spectral clustering technique has few fundamental advantages: (i) it is simple to implement, (ii) it can be solved efficiently, and, (iii) it delivers better clustering results. These inherent advantages of spectral clustering technique justify its usage in our work.

In spectral clustering, the graph partitions are derived based on the spectrum of the similarity matrix (also called the affinity matrix) associated with the given graph. In this paradigm, the $(i, j)^{\text{th}}$ element of the similarity matrix (denoted by $s_{ij} \geq 0$) will represent the similarity between the i^{th} node and the j^{th} node of the given graph. In terms of the similarity values, the spectral clustering algorithm can be seen as a clustering method which seeks to partition the graph such that nodes in different partitions have a low similarity value between them while the nodes in the same partition have a higher similarity value between them.

Remark 3. In a typical data-point clustering application, the graph representation of the data-points is a result of similarity values between the data-points (not the other way around as described above). In there, $(i, j)^{\text{th}}$ element of the similarity matrix represents the similarity between i^{th} and j^{th} data-points. Therefore, a weighted graph (called a similarity graph) can be constructed to represent these inter data-point similarities, where each node represents a data-point, and the edge weights are the corresponding similarity values.

Construction of the similarity matrix: In our application, the target topology $\mathcal{G} = (\mathcal{V}, \mathcal{E})$ along with target parameters are a given. Therefore, the next step is to construct an effective similarity matrix to represent this given information. For that, we need to define a similarity measure between all the target pairs. Let us denote the similarity between targets $i, j \in \mathcal{V}$ as $s_{ij} \geq 0$ where,

$$s_{ij} = \exp\left(-\frac{|d(i, j)|^2}{2\sigma^2}\right). \quad (47)$$

This is known as the Gaussian similarity function where $d : \mathcal{V} \times \mathcal{V} \rightarrow \mathbb{R}$. Specifically, $d(i, j)$ represents a disparity metric between the targets i and j while the parameter σ controls the width of the neighborhoods. According to (47), when the disparity between two targets is higher, the respective similarity measure would be smaller and vice versa. Now, the next step would be to define a good disparity metric for the class of persistent monitoring problems.

Remark 4. Using the physical distance as the disparity metric (i.e., $d(i, j) = \|X_i - X_j\|$) is not accurate because, even if two targets i and j are located nearby, there might not be a direct path segment between them (i.e., $(i, j) \notin \mathcal{E}$). This suggests an alternative disparity metric: $d(i, j) = d_{SP}(i, j) = \text{shortest path length between target } i \text{ and target } j$. However, this metric also falls short of providing a good characterization for the underlying persistent monitoring aspects of the problem. This is because it ignores any effects resulting from the intermediate targets in the shortest path. For example, in a specific shortest path, if there are a lot of intermediate targets or, if there are one/few intermediate targets with relatively higher uncertainty rates, then, it should affect the disparity value regardless of the shortest path distance.

Taking the remark 4 into account, we propose a novel disparity metric called *minimum mean covering cycle uncertainty* (CC),

$$d(i, j) = d_{CC}(i, j) = \min_{\Xi: i, j \in \Xi} J_{ss}(\Xi). \quad (48)$$

The argmin of the above problem is denoted as Ξ_{ij}^* and, is defined as the *optimum covering cycle* (OCC) for the target pair i and j . If the inter-target available path segments in \mathcal{E} are linear, it can be shown that for any $(i, j) \in \mathcal{E}$, the corresponding OCC is $\Xi_{ij}^* = \{i, j\}$.

In other words, the OCC Ξ_{ij}^* provides the best way (at steady state) to cover the two given targets i and j in a single target-cycle. The corresponding CC-value $d_{CC}(i, j)$ is the steady state mean cycle uncertainty $J_{ss}(\Xi_{ij}^*)$. Therefore, if the CC value is higher for a certain target pair, it implies that it is difficult to cover those two targets in a single target-cycle, and, vice versa. Thus, it is clear that this disparity metric $d_{CC}(i, j)$ does a better job in providing a good characterization for the underlying persistent monitoring aspects of the problem configuration - compared to the other two disparity metrics suggested in remark 4.

In order to compute the proposed disparity metric $d_{CC}(i, j)$, $\forall i, j \in \mathcal{V}$, we propose the Algorithm 5 which is a modified version of the famous Dijkstra's algorithm [27] coupled with cycle expanding and refining techniques discussed in section IV. Disparity metric values given by Algorithm 5 are then used in (47) to compute the similarity values: $s_{ij} \forall i, j \in \{1, 2, \dots, M\}$. Note that the neighborhood width parameter was chosen as $\sigma = \frac{1}{3}(0.7d_{CC}^{min} + 0.3d_{CC}^{max})$ where d_{CC}^{min} and d_{CC}^{max} respectively corresponds to the minimum and maximum disparity values observed. Subsequently, the obtained inter-target similarity values are used to form the similarity matrix S where,

$$S = [\{s_{ij}\}_{\forall(i,j)}] \in \mathbb{R}^{M \times M}.$$

Algorithm 5 Modified Dijkstra's algorithm used to find the proposing disparity metric values: $d_{CC}(i, j) \forall j \in \mathcal{V}$

- 1: **Input:** A start node i , Target topology $G = (\mathcal{V}, \mathcal{E})$.
 - 2: **Output:** $d_{CC}(i, j)$, $\forall j \in \mathcal{V}$.
 - 3: $V := \emptyset$; $U := \mathcal{V}$; ▷ Visited/unvisited target sets.
 - 4: $C_{CC}(j) := \{\}$, $\forall j \in \mathcal{V}$; ▷ Null cycles.
 - 5: $C_{CC}(i) := \{i\}$; ▷ A cycle with only i on it.
 - 6: $J_{CC}(j) := \infty$, $\forall j \in \mathcal{V}$; $J_{CC}(i) := 0$; ▷ CC values.
 - 7: **while** $U \neq \emptyset$ **do** ▷ Till all targets get their own OCC.
 - 8: $j^* := \arg \min_{j: j \in U} J_{CC}(j)$;
 - 9: $\Xi_{ij^*}^* := C_{CC}(j^*)$;
 - 10: $V := V \cup j^*$; $U := U \setminus j^*$; ▷ j^* got its own OCC.
 - 11: **for** $k \ni (j^*, k) \in \mathcal{E}$ **do**
 - 12: $\Xi_{ik}^* :=$ when $\Xi_{ij^*}^*$ expanded (and then refined) to include target k in the best way out of three TCEOs discussed;
 - 13: **if** $J_{CC}(k) > J_{ss}(\Xi_{ik}^*)$ **then** ▷ Found a better OCC!
 - 14: $C_{CC}(k) := \Xi_{ik}^*$; ▷ OCC updated.
 - 15: $J_{CC}(k) := J_{ss}(\Xi_{ik}^*)$; ▷ CC updated.
 - 16: **end if**
 - 17: **end for**
 - 18: **end while**
 - 19: **Return** $J_{CC}(j)$, $\forall j \in \mathcal{V}$;
-

Spectral clustering algorithm: In the process of spectral clustering, computation of 'Weighted Adjacency Matrix (W)'

and 'Degree Matrix (D)' is done using the obtained similarity matrix S . Then, those matrices are used to compute the Laplacian matrix L (unnormalized) corresponding to the similarity matrix S .

In literature, often the similarity matrix refers to a matrix with disparity values $d(i, j)$ as its elements. However, we have constructed the similarity matrix S by directly transforming the disparity values got via Algorithm 5 using (47). Therefore, in our case, the weighted adjacency matrix is the similarity matrix. Thus,

$$W = [\{w_{ij}\}_{\forall(i,j)}] = S = [\{s_{ij}\}_{\forall(i,j)}] \in \mathbb{R}^{M \times M}. \quad (49)$$

The degree matrix D is obtained using the elements of W as,

$$D = \text{diag}([d_1, d_2, \dots, d_M]^T); \text{ with } d_i = \sum_{j=1}^M w_{ij}. \quad (50)$$

The unnormalized Laplacian matrix L is then computed as,

$$L = D - W. \quad (51)$$

It should be noted that there are variants of the spectral clustering algorithm which uses normalized Laplacian matrices denoted by L_{sym} and L_{rw} as opposed to using L [26]. Here,

$$L_{sym} = D^{-\frac{1}{2}} L D^{-\frac{1}{2}}, \quad (52)$$

$$L_{rw} = D^{-1} L. \quad (53)$$

In our work, we use the normalized spectral clustering method proposed in [28], which utilizes the normalized Laplacian L_{rw} . We chose this method because it has a somewhat relatable (to persistent monitoring) interpretation based on random walks on the similarity graph. Specifically, a random walk on a graph can be seen as a stochastic process where an agent randomly jumps from vertex to vertex. The normalized spectral clustering method proposed in [28] can be interpreted as trying to find a partition of the similarity graph such that the random walk stays long within the same cluster and seldom jumps between clusters.

Algorithm 6 outlines the normalized spectral clustering procedure (based on [28]) to get the target clusters $\mathcal{V}_1, \mathcal{V}_2, \dots, \mathcal{V}_N$. Each target cluster \mathcal{V}_a can then be used to form a sub-graph out of the given target topology $\mathcal{G} = (\mathcal{V}, \mathcal{E})$ as $\mathcal{G}_a = (\mathcal{V}_a, \mathcal{E}_a)$ where $\mathcal{E}_a \subseteq \mathcal{E}$ is the set of intra-cluster edges taken from complete set of edges \mathcal{E} , $\forall a \in \{1, 2, \dots, N\}$. Note that the set of inter-cluster edges (i.e., $\mathcal{E}^I = \mathcal{E} \setminus \cup_{a=1}^N \mathcal{E}_a$) are now not included in any of the formed sub-graphs.

C. Balancing the obtained graph partitions

Once the sub-graphs are formed, as suggested in step 4 of the complete solution procedure given in Algorithm 4, we follow the refined sub-optimal target-cycle construction procedure (discussed in section IV) for each sub-graph. The resulting cycle for a sub-graph \mathcal{G}_a is denoted as Ξ_a . For notational convenience, let's assume that agent $a \in \mathcal{A}$ is the assigned agent to monitor the target topology in sub-graph \mathcal{G}_a . This assumption is relieved later on.

The obtained set of clusters is called *balanced* if the steady state mean cycle uncertainties $J_{ss}(\Xi_a)$ (on the sub-graph \mathcal{G}_a by

Algorithm 6 Normalized Spectral Clustering [28]

-
- 1: **Input:** Normalized Laplacian L_{rw} .
 - 2: **Output:** Target clusters $\mathcal{V}_1, \mathcal{V}_2, \dots, \mathcal{V}_N$.
 - 3: Compute the first N eigenvectors u_1, u_2, \dots, u_N of L_{rw} .
 - 4: Let $U \in \mathbb{R}^{N \times M}$ be the matrix containing u_1, u_2, \dots, u_N as columns.
 - 5: For $i = 1, \dots, M$ let $y_i \in \mathbb{R}^N$ be the vector corresponding to the i^{th} row of U .
 - 6: Cluster the data points $\{y_i\}_{i=1, \dots, M} \in \mathbb{R}^N$ using a k-means algorithm (where $k = N$) into N clusters C_1, \dots, C_N .
 - 7: **Return** Target clusters $\mathcal{V}_1, \mathcal{V}_2, \dots, \mathcal{V}_N$ with $\mathcal{V}_i = \{j : j \ni y_j \in C_i\}$
-

agent a) are approximately identical for all $a \in \mathcal{A}$. Despite the dependence on the nature of the given target topology \mathcal{G} , the spectral clustering method is often able to provide a balanced set of clusters. However, when this is not the case, it is intuitive to think of an inter-cluster target exchange scheme - which aims to balance the set of clusters by iteratively modifying them.

Note that such a target exchange operation between two given clusters will affect the constructed target-cycles on those clusters. However, since we can evaluate the steady state performance of target-cycles, we can use this knowledge to identify globally beneficial inter-cluster target exchange operations.

This process can also be seen as a situation where N agents (i.e., \mathcal{A}) trying to exchange their owned set of resources (i.e., the targets) among each other so that a global objective (i.e., $\sum_{a=1}^N J_{ss}(\Xi_a)$) is minimized. Note that, in our case, each cluster is assigned to an agent. Therefore, we can think of the cluster changes as decisions taken by the assigned agent.

In such a paradigm, note that the net global effect of a target exchange operation between two neighboring agents (i.e., neighboring clusters) can be independently (from others) computed. Therefore, a distributed greedy algorithm is proposed here to search and execute globally beneficial target exchange operations iteratively. An iteration of the proposed algorithm for a generic agent $a \in \mathcal{A}$ is given in Algorithm 7.

Note that, when the agent $a \in \mathcal{A}$ wants to expand its cluster \mathcal{V}_a by adding a new target i to it, he needs to choose the most beneficial target-cycle expansion operation out of the three discussed TCEOs to expand Ξ_a so that it includes the target i (See step 3 and 18 in Algorithm 7 - also similar to step 12 of Algorithm 5). In contrast, when an agent $a \in \mathcal{A}$ wants to remove a target i from its cluster \mathcal{V}_a , he needs to recompute his target-cycle completely on $\mathcal{V}_a \setminus \{i\}$ (See step 9 and 22 of Algorithm 7).

In all, the proposing Algorithm 7 helps to balance/distribute the persistent monitoring load among the agents (clusters) uniformly. This load balancing technique also relieves the need to have a properly chosen neighborhood width parameter σ in (47) for the spectral clustering. Also, since the cluster modifications (step 18 and 22) are carried out when only they lead to global cost improvement, the given algorithm should converge after a finite number of iterations. Specifically, the

convergence criterion is the event where all the agents fail to find a feasible solution to the step 12 of Algorithm 7.

Algorithm 7 An iteration of the proposed post target cluster/cycle refinement algorithm:

-
- 1: **Input:** Agent a 's initial target cluster and the target-cycle: $\{\mathcal{V}_a, \Xi_a\}$
 - 2: **for** each (neighbor) $T_i \notin \mathcal{V}_a$ but $T_i \in \mathcal{V}_b$ **do**
 - 3: Find the best way to append T_i to Ξ_a
 - 4: **Store:** $(J_{a,i}^A, \Xi_{a,i}^A) :=$ resulting gain and the cycle;
 - 5: **Offer:** $f_{a,i} : \{a, T_i, J_{a,i}^A\}$ to agent b **if** $J_{a,i}^A > 0$.
 - 6: **end for**
 - 7: —
 - 8: **for** each $T_i \in \Xi_a$ with an external offer **do**
 - 9: Recompute a new cycle on $\mathcal{V}_a \setminus \{T_i\}$ (detaching).
 - 10: **Store:** $(J_{a,i}^D, \Xi_{a,i}^D) :=$ resulting gain and the cycle;
 - 11: **end for**
 - 12: Best offer: $f_{b^*,i} : \arg \max_{(b,i): J > 0} J = J_{b^*,i}^{Net} = (J_{b^*,i}^A + J_{a,i}^D)$
 - 13: **Acknowledge** $Ack_{b^*,a,i} = \{b^*, a, T_i, J_{b^*,a,i}^{Net}\}$ to b^* .
 - 14: —
 - 15: Best acknowledgement received: $Ack_{a,c^*,i}$ (valued $J_{a,c^*,i}^{Net}$).
 - 16: **if** $J_{a,c^*,i}^{Net} > J_{b^*,a,i}^{Net}$ **then** \triangleright Received Ack is better than sent.
 - 17: **if** agent c^* has no other commitments **then**
 - 18: $\mathcal{V}_a := \mathcal{V}_a \cup \{i\}$; (also update Ξ_a). \triangleright Appended i .
 - 19: **end if**
 - 20: **else if** $J_{a,c^*,i}^{Net} < J_{b^*,a,i}^{Net}$ **then** \triangleright Sent Ack is better.
 - 21: **if** Agent b^* has no other commitments **then**
 - 22: $\mathcal{V}_a := \mathcal{V}_a \setminus \{i\}$; (also update Ξ_a). \triangleright Detached i .
 - 23: **end if**
 - 24: **end if**
-

D. Re-assigning agents to clusters

According to the problem formulation presented in section II, each agent a has a pre-specified initial location $s_a(0)$ ($\forall a \in \mathcal{A}$). However, up to now, we haven't used this information in our analysis. So far, we have used the given target topology \mathcal{G} to create a balanced set of sub-graphs and, within each sub-graph we have found a refined sub-optimal target-cycle Ξ_b for an agent to cover ($\forall b \in \{1, 2, \dots, N\}$). Therefore, our next step is to assign each agent a with one of the found target-cycles Ξ_b where $a, b \in \{1, 2, \dots, N\}$.

First, we define the assignment cost between an agent a and a target-cycle Ξ_b as w_{ab} where $w_{ab} = \{\text{Starting from } s_a(0), \text{ the shortest available path length to reach any one of the targets in } \Xi_b\}$. Then, we use the Dijkstra's shortest path algorithm [27] to compute all the assignment weights. Next, we utilize the standard linear assignment problem solving technique: the shortest augmenting path algorithm [27] to find the optimal set of assignments. The optimal total assignment cost corresponds to the total distance that the agents have to travel before ending up in their designated target-cycles.

Threshold control policy $\Theta^{(0)}$ selection: Let us assume agent $a \in \mathcal{A}$ is optimally assigned to the target-cycle Ξ_b , and, the corresponding shortest path from $s_a(0)$ to any one of the targets in Ξ_b is $\Phi_{ab} = \{i_1, i_2, \dots, i_n\}$. Taking $\Phi'_{ab} = \Phi_{ab} \setminus \{i_n\}$, note that $\Phi'_{ab} \cap \Xi_b = \{i_n\}$, $i_n \in \Xi_b$, and, $X_{i_n} \equiv s_a(0)$.

Recall that we need to use the Algorithm 2 with the target-cycle Ξ_b to set the initial threshold matrix of agent a (i.e., $\Theta^{a(0)}$). However, Algorithm 2 only assigns the set of rows: $\{j : j \in \Xi_b\}$ of $\Theta^{a(0)}$ (See step 4). Therefore, to make sure that agent a follows the path Φ_{ab} , we also have to assign the set of rows: $\{j : j \in \Phi'_{ab}\}$ of $\Theta^{a(0)}$.

Specifically, if j and k are two consecutive entries in Φ_{ab} , we need to set $(j, j)^{\text{th}}$ and $(j, k)^{\text{th}}$ entries of $\Theta^{a(0)}$ to 0. As per the remaining entries of the j^{th} row: if $(j, l) \in \mathcal{E}$, we need to set the $(j, l)^{\text{th}}$ entry to P , otherwise to ∞ . Note that P is a large number, previously defined in the discussion of Algorithm 2. An example case is illustrated in Fig. 27.

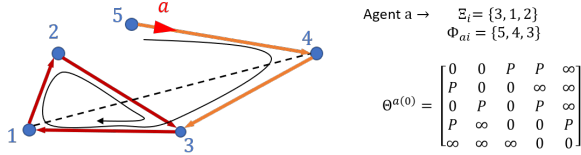


Fig. 27: The generated initial threshold matrix $\Theta^{a(0)}$ when the agent a is initially at target 5 (i.e., $s_a(0) = X_5$), assigned to the target-cycle $\Xi_i = \{3, 1, 2\}$, with the shortest path leading to Ξ_i as $\Phi_{ai} = \{5, 4\}$.

With this, we now have discussed all the steps involved in the overall solution procedure (outlined in Algorithm 4) that we propose for the persistent monitoring problems on graphs.

E. Simulation results

Effect of graph partitioning: First, we illustrate the effect of graph partitioning by considering the multi-agent simulation example MASE1 given in Fig. 4 along with three new such examples named MASE2, MASE3, and MASE4 given in Fig. 28, 29 and 30 respectively. Note that in MASE2, only two agents are deployed whereas, in the other three configurations, three agents are deployed. Also, note that when the initial TCP $\Theta^{(0)}$ is chosen randomly, the gradient steps have converged to TCPs with J_T values 270.2, 91.7, 274.0, and 201.3 respectively in each MASE.

Now, when the proposing graph partitioning techniques is applied to each graph (i.e., the step 3 of Algorithm 4), sub-graphs shown in Fig. 31 are formed. Fig. 32 shows the generated constrained target-cycles (in red color) within each of the formed sub-graphs under each MASE (i.e., the step 4 of Algorithm 4). Next, to highlight sole effect of graph partitioning, we skip the graph partitioning refinements (i.e., the step 5 of Algorithm 4) and continue to generate suitable initial TCPs (i.e., steps 6 and 7 in Algorithm 4). Finally, when the generated initial TCPs were used in gradient descent (8) (i.e., step 8 in Algorithm 4), the observed optimal TCPs had the J_T values as 112.9, 45.2, 62.5 and 63.7 respectively. Fig. 32 shows the terminal (i.e., at $t = T$) conditions of the problem configurations under these optimal TCPs. The respective overall improvements achieved from deploying the proposing initialization technique are: +157.3 (58.2%), +46.5 (50.7%), +211.5 (77.2%), and +137.6 (68.4%). Therefore, it is clear that the proposing graph

partitioning based method (even without graph partitioning refinements) is capable of delivering much improved solutions.

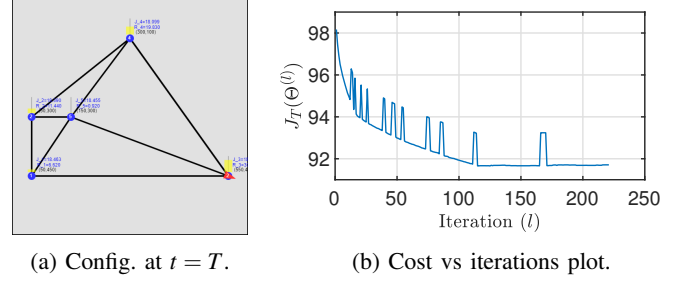


Fig. 28: Multi-agent simulation example 2 (MASE2): Starting with a random $\Theta^{(0)}$, converged to a TCP with the cost $J_T = 91.7$.

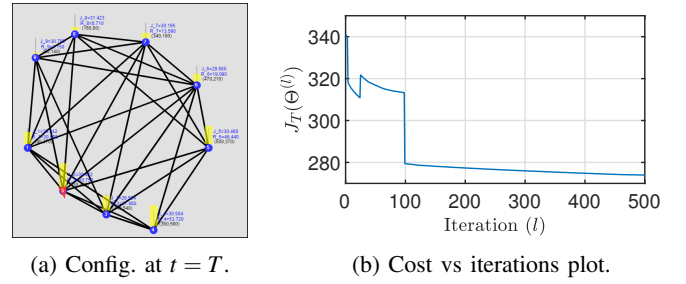


Fig. 29: Multi-agent simulation example 3 (MASE3): Starting with a random $\Theta^{(0)}$, converged to a TCP with the cost $J_T = 274.0$.

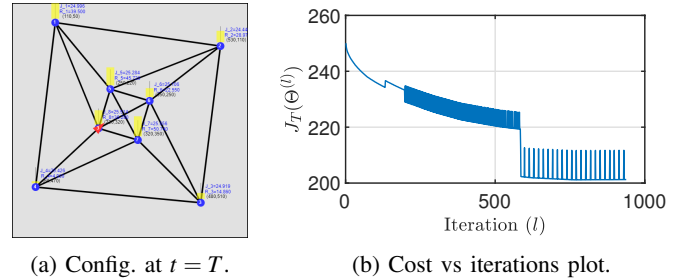


Fig. 30: Multi-agent simulation example 4 (MASE4): Starting with a random $\Theta^{(0)}$, converged to a TCP with the cost $J_T = 201.3$.

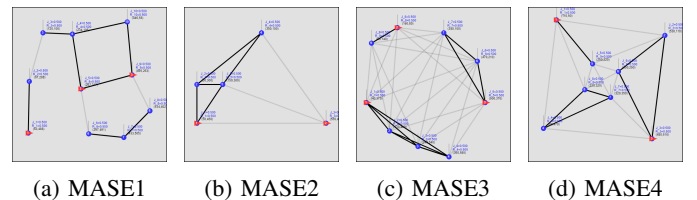


Fig. 31: Clustering results obtained for the considered MASEs.

Effect of graph partitioning refinements: As the next step, we illustrate the effect of graph partitioning refinements (i.e., the step 5 of Algorithm 4) using the MASE1. Fig. 33

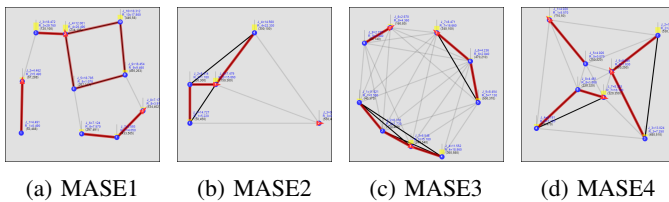


Fig. 32: Target-cycles formed on each sub-graphs (red colored contours). The configurations have been drawn at $t = T$ under the optimal TCPs found using Algorithm 4 with its step 5 skipped (i.e., the graph partitioning refinement step). Respective cost (improvement) values compared to Fig. 4, 28, 29 and 30: 112.9 (+157.3), 45.2 (+46.5), 62.5, (+211.5) and 63.7 (+137.6)

shows the evolution of graph partitions (and the respective target-cycles) through two graph partitioning refinement steps (also called inter-cluster target exchange steps). However, in there, we have used an appropriately computed neighborhood width parameter value ($\sigma = 32.9$) in (47) to obtain the initial graph partitions shown in Fig. 33(a).

However, Fig. 34(a) shows a situation where the initial graph partitions have been obtained using a poorly chosen σ value ($\sigma = 7.67$). The subsequent partitioning refinement steps are shown in Fig. 34(b)→(f). Notice that terminal set of graph partitions shown in Fig. 33(d) and Fig. 34(f) are identical. Therefore, it illustrates the fact that we can start with a poor set of initial graph partitions and improve upon them iteratively to get to a better set of graph partitions, using the introduced graph partitioning refinement steps (i.e., the Algorithm 7).

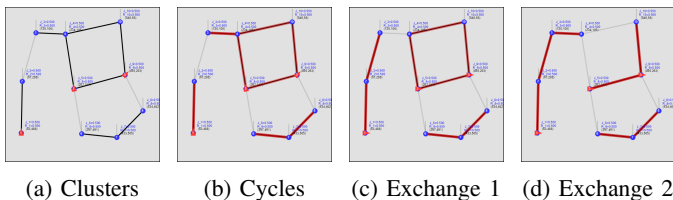


Fig. 33: MASE1: (a) Clustering result obtained (with a properly chosen σ value), (b) Constrained cycles generated on each sub-graph using Algorithm 3, (c),(d) Two inter-cluster target exchange steps, and, (d) Best target-cluster/cycle arrangement found for the MASE1.

Effect of the proposing (complete) initialization scheme (Algorithm 4): We investigate the effect of the complete proposing initialization scheme (given in Algorithm 4) using the four multi-agent simulation examples: MASE1, MASE2, MASE3 and MASE4. Sub-figure (a) of Fig. 35, 36, 37, and, 38 shows the determined graph partitions (and the derived target-cycles) of each considered problem configuration. Sub-figure (b) of each of those figures shows that the initial TCP obtained using the derived target-cycles have J_T values 90.9, 35.1, 59.5 and 59.8 respectively. Same figures show that these J_T values cannot be further improved using the gradient steps (8). To ensure these initial TCPs are locally optimal, in each case, at $l = 100$, the derived initial TCP (i.e., $\Theta^{(0)}$) was

TABLE I: Summary of the results obtained for the considered simulation examples

Cost of the optimal TCP Θ^* (found using (8)): $J_T(\Theta^*)$	Single Agent Simulation Examples			Multi-Agent Simulation Examples			
	1	2	3	1	2	3	4
With randomly generated initial TCP $\Theta^{(0)}$	129.2	651.3	497.9	270.2	91.7	274.0	201.3
With initial TCP $\Theta^{(0)}$ given by the proposing Algorithm 4	114.6	567.0	449.5	90.9	35.1	59.5	59.8
Percentage improvement (%)	10.7	12.9	9.7	66.3	61.7	78.2	70.3

randomly perturbed. The subsequent observations shows that $\Theta^{(l)}$ converges back to the same initial TCP found in each case.

It is important to note that these solutions are much better than the best TCPs obtained with random initialization of $\Theta^{(0)}$ (shown in Fig. 4, 28, 29, and 30). The improvement margins of the four considered examples are by: +179.3 (66.3%), +56.6 (61.7%), +214.5 (78.2%), and +141.5 (70.3%). All the discussed simulation results have been summarized in the Table I.

Also, note that, when compared to the performance of the target-cycles shown in Fig. 32 (where initial graph partitions were not further refined), the improvement margins of the four considered examples (of the respective complete solutions) are by: +22.0 (19.4%), +10.1 (22.3%), +3 (0.48%), and +3.9 (6.12%). These achieved improvement levels emphasize the importance of the proposed graph partition refinement step.

As the last step, we consider a new set of multi-agent simulation examples labeled MASE5 - MASE12, as shown in Fig. 39. In each case $N = 3$ and $M = 15$ have been used. Further, each underlying target topology has been generated randomly - as a random geometric graph [29] with communication range parameter $r = 200$. When the proposing greedy initialization technique is deployed, the obtained new terminal solutions are shown in Fig. 40. Across all these eight cases, the average improvement achieved is +315.7 (69.1%).

In simulation examples MASE5 - MASE12, on an Intel® Core™ i7-7800 CPU 3.20 GHz Processor with a 32 GB RAM, the average execution time observed for the proposing greedy initialization technique (i.e., to Algorithm 4 to generate $\Theta^{(0)}$) was 13.7s. Also, all such generated initial TCPs were found to be locally optimal (Similar to what we saw in MASE1-MASE4). However, when initialized with a randomly chosen TCP $\Theta^{(0)}$, the average execution time observed for the subsequent convergence of the gradient steps in (8) was 245.8s. Therefore, the execution time taken for the proposing offline greedy initialization process is much smaller, and, at the same time, it is highly effective.

Finally, we recall that all the simulation examples discussed were evaluated on the developed JavaScript based simulator, which is made available at <http://www.bu.edu/codes/simulations/shiran27/PersistentMonitoring/>. Readers are invited to reproduce the reported results and also to try new problem configurations with customized problem parameters, using the developed interactive simulator.

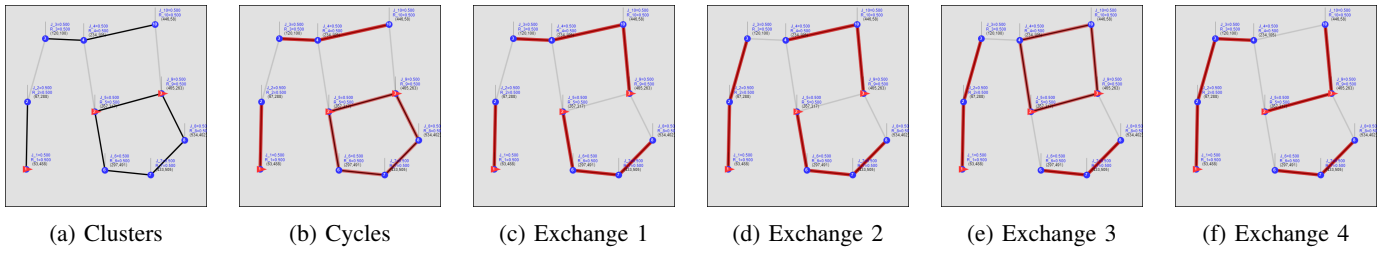


Fig. 34: MASE1: (a) Clustering result obtained (with a poorly chosen σ value), (b) Constrained cycles generated on each sub-graph using Algorithm 3, (c),(d),(e),(f) Four inter-cluster target exchange steps, and, (f) Best target-cluster/cycle arrangement found for the MASE1. (same as in Fig. 33(d)).

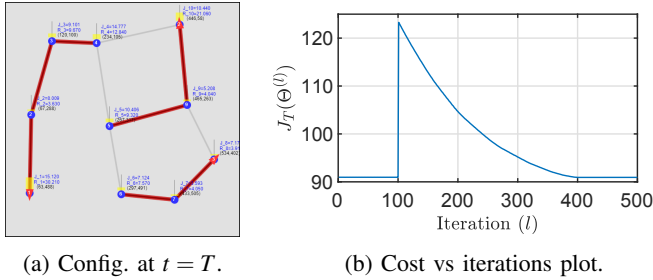


Fig. 35: MASE1: The TCP $\Theta^{(0)}$ given by the identified cycles (the red traces in (a)) shows local optimality. At $l = 100, \Theta^{(l)}$ is randomly perturbed. Yet, converges back to the initial TCP. Cost $J_T = 90.9$ (Improvement = +179.3 compared to Fig. 4).

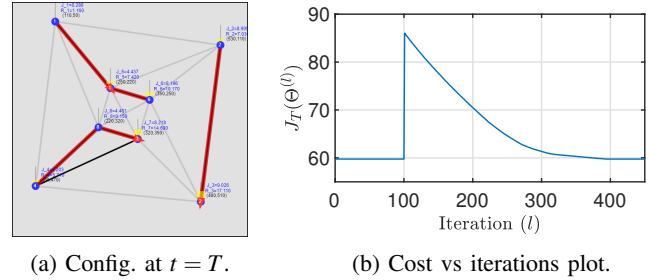


Fig. 38: MASE4: The TCP $\Theta^{(0)}$ given by the identified cycles (the red traces in (a)) shows local optimality. At $l = 100, \Theta^{(l)}$ is randomly perturbed. Yet, converges back to the initial TCP. Cost $J_T = 59.8$ (Improvement = +141.5 compared to Fig. 30).

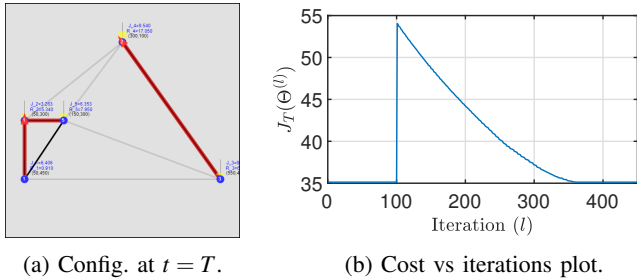


Fig. 36: MASE2: The TCP $\Theta^{(0)}$ given by the identified cycles (the red traces in (a)) shows local optimality. At $l = 100, \Theta^{(l)}$ is randomly perturbed. Yet, converges back to the initial TCP. Cost $J_T = 35.1$ (Improvement = +56.6 compared to Fig. 28).

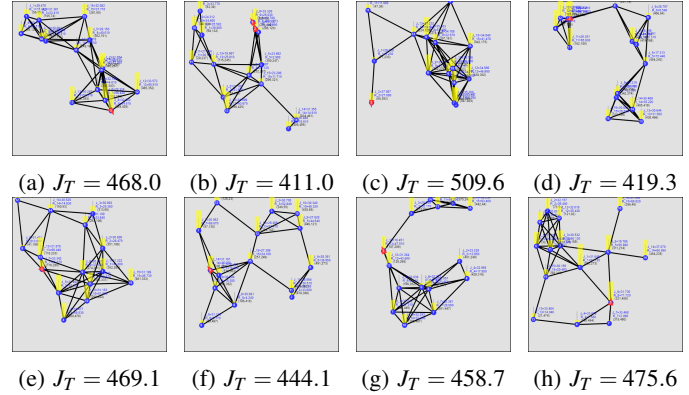


Fig. 39: Problem configurations MASE5 - MASE12 and their respective cost values under the optimal TCP Θ^* found using (8) when started with a randomly chosen $\Theta^{(0)}$.

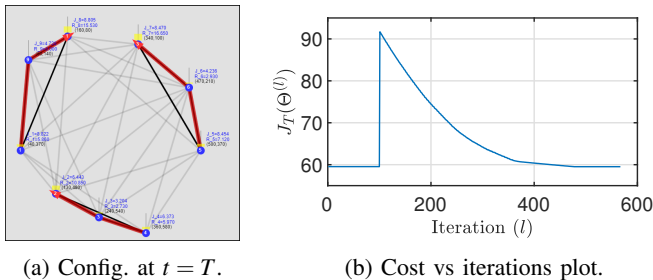


Fig. 37: MASE3: The TCP $\Theta^{(0)}$ given by the identified cycles (the red traces in (a)) shows local optimality. At $l = 100, \Theta^{(l)}$ is randomly perturbed. Yet, converges back to the initial TCP. Cost $J_T = 59.5$ (Improvement = +214.5 compared to Fig. 29).

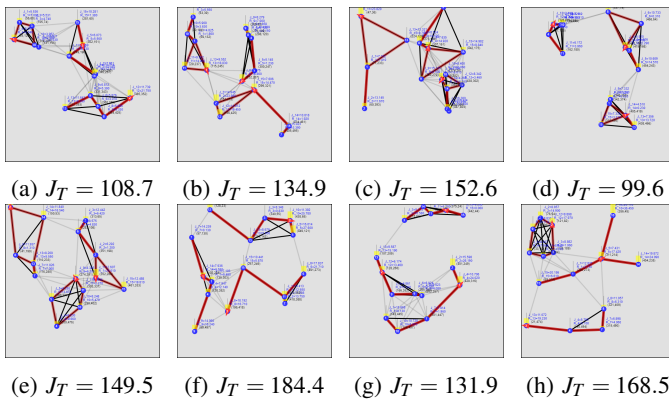


Fig. 40: Problem configurations MASE5 - MASE12 and their respective cost values under the optimal TCP Θ^* found using (8) when started with $\Theta^{(0)}$ given by proposing Algorithm 4.

VI. CONCLUSION

We have considered the optimal multi-agent persistent monitoring problem on a set of targets interconnected according to a fixed graph topology. We have adopted a class of distributed threshold-based parametric controllers where IPA can be used to determine optimal threshold parameters in an on-line manner using gradient descent. Due to the non-convex nature of the problem, optimal thresholds given by gradient descent highly depend on the used initial thresholds. To address this issue, the asymptotic steady-state behavior of the persistent monitoring system is studied extensively, leading to a computationally efficient and effective threshold initialization scheme. An interesting future work would be to conduct an asymptotic analysis of persistent monitoring systems where agents are allowed to share targets, and then to use the obtained theoretical results to further improve the proposed threshold initialization scheme.

REFERENCES

- [1] M. Zhong and C. G. Cassandras, "Distributed Coverage Control and Data Collection With Mobile Sensor Networks," *IEEE Trans. on Automatic Control*, vol. 56, no. 10, pp. 2445–2455, 2011.
- [2] S. Su and Z. Lin, "Distributed Consensus Control of Multi-agent Systems with Higher Order Agent Dynamics and Dynamically Changing Directed Interaction Topologies," *IEEE Trans. on Automatic Control*, vol. 61, no. 2, pp. 515–519, 2015.
- [3] V. A. Huynh, J. J. Enright, and E. Frazzoli, "Persistent patrol with limited-range on-board sensors," in *49th IEEE Conf. on Decision and Control*, 2010, pp. 7661–7668.
- [4] X. Lin and C. G. Cassandras, "An optimal control approach to the multi-agent persistent monitoring problem in two-dimensional spaces," *IEEE Trans. on Automatic Control*, vol. 60, no. 6, pp. 1659–1664, dec 2015.
- [5] D. Aksaray, K. Leahy, and C. Belta, "Distributed Multi-Agent Persistent Surveillance Under Temporal Logic Constraints," *IFAC-PapersOnLine*, vol. 48, no. 22, pp. 174–179, jan 2015.
- [6] N. Michael, E. Stump, and K. Mohta, "Persistent surveillance with a team of MAVs," in *IEEE Intl. Conf. on Intelligent Robots and Systems*, sep 2011, pp. 2708–2714.
- [7] J. Trevathan and R. Johnstone, "Smart environmental monitoring and assessment technologies (Semat)a new paradigm for low-cost, remote aquatic environmental monitoring," *Sensors (Switzerland)*, vol. 18, no. 7, jul 2018.
- [8] C. G. Cassandras, X. Lin, and X. Ding, "An optimal control approach to the multi-agent persistent monitoring problem," *IEEE Trans. on Automatic Control*, vol. 58, no. 4, pp. 947–961, apr 2013.
- [9] N. Zhou, X. Yu, S. B. Andersson, and C. G. Cassandras, "Optimal Event-Driven Multiagent Persistent Monitoring of a Finite Set of Data Sources," *IEEE Trans. on Automatic Control*, vol. 63, no. 12, pp. 4204–4217, dec 2018.
- [10] S. L. Smith, M. Schwager, and D. Rus, "Persistent monitoring of changing environments using a robot with limited range sensing," in *IEEE Intl. Conf. on Robotics and Automation*. IEEE, may 2011, pp. 5448–5455.
- [11] Y. Khazaeni and C. G. Cassandras, "Event-driven trajectory optimization for data harvesting in multiagent systems," *IEEE Trans. on Control of Network Systems*, vol. 5, no. 3, pp. 1335–1348, sep 2018.
- [12] X. Meng, A. Houshmand, and C. G. Cassandras, "Hybrid System Modeling of Multi-Agent Coverage Problems with Energy Depletion and Repletion," *IFAC-PapersOnLine*, vol. 51, no. 16, pp. 223–228, 2018.
- [13] Z. Shen and S. B. Andersson, "Tracking nanometer-scale fluorescent particles in two dimensions with a confocal microscope," *IEEE Trans. on Control Systems Technology*, vol. 19, no. 5, pp. 1269–1278, sep 2011.
- [14] C. G. Cassandras, Y. Wardi, C. G. Panayiotou, and C. Yao, "Perturbation Analysis and Optimization of Stochastic Hybrid Systems," *European Journal of Control*, vol. 16, no. 6, pp. 642–661, jan 2010.
- [15] N. Zhou, C. G. Cassandras, X. Yu, and S. B. Andersson, "Optimal Threshold-Based Distributed Control Policies for Persistent Monitoring on Graphs," in *American Control Conference*, 2019, pp. 2030–2035.
- [16] X. Yu, S. B. Andersson, N. Zhou, and C. G. Cassandras, "Optimal dwell times for persistent monitoring of a finite set of targets," in *American Control Conference*, may 2017, pp. 5544–5549.
- [17] T. Bektas, "The multiple traveling salesman problem: An overview of formulations and solution procedures," *Omega*, vol. 34, no. 3, pp. 209–219, jun 2006.
- [18] N. Zhou, C. G. Cassandras, X. Yu, and S. B. Andersson, "Optimal Threshold-Based Control Policies for Persistent Monitoring on Graphs," mar 2018. [Online]. Available: <http://arxiv.org/abs/1803.02798>
- [19] C. G. Cassandras and S. LaFortune, *Introduction to Discrete Event Systems*, 2nd ed. Springer Publishing Company, Inc., 2010.
- [20] H. Flanders, "Differentiation Under the Integral Sign," *The American Mathematical Monthly*, vol. 80, no. 6, pp. 615–627, 1973.
- [21] D. P. Bertsekas, *Nonlinear Programming*. Athena Scientific, 2016.
- [22] K. S. Miller, "On the Inverse of the Sum of Matrices," *Mathematics Magazine*, vol. 54, no. 2, p. 67, mar 1981.
- [23] N. Bof, R. Carli, and L. Schenato, "Lyapunov Theory for Discrete Time Systems," sep 2018. [Online]. Available: <http://arxiv.org/abs/1809.05289>
- [24] A. Blazinskas and A. Misevicius, "Combining 2-Opt, 3-Opt and 4-Opt with K-Swap-Kick Perturbations for the Travelling Salesman Problem," Tech. Rep., 2011.
- [25] C. Nilsson, "Heuristics for the Traveling Salesman Problem," Tech. Rep., 2003.
- [26] U. von Luxburg, "A Tutorial on Spectral Clustering," nov 2007. [Online]. Available: <http://arxiv.org/abs/0711.0189>
- [27] R. K. Ahuja, T. L. Magnanti, and J. B. Orlin, *Network flows : theory, algorithms, and applications*. Prentice Hall, 1993.
- [28] Jianbo Shi and J. Malik, "Normalized cuts and image segmentation," *IEEE Trans. on Pattern Analysis and Machine Intelligence*, vol. 22, no. 8, pp. 888–905, 2000.
- [29] J. Dall and M. Christensen, "Random geometric graphs," *Physical Review E - Statistical Physics, Plasmas, Fluids, and Related Interdisciplinary Topics*, vol. 66, no. 1, mar 2002.